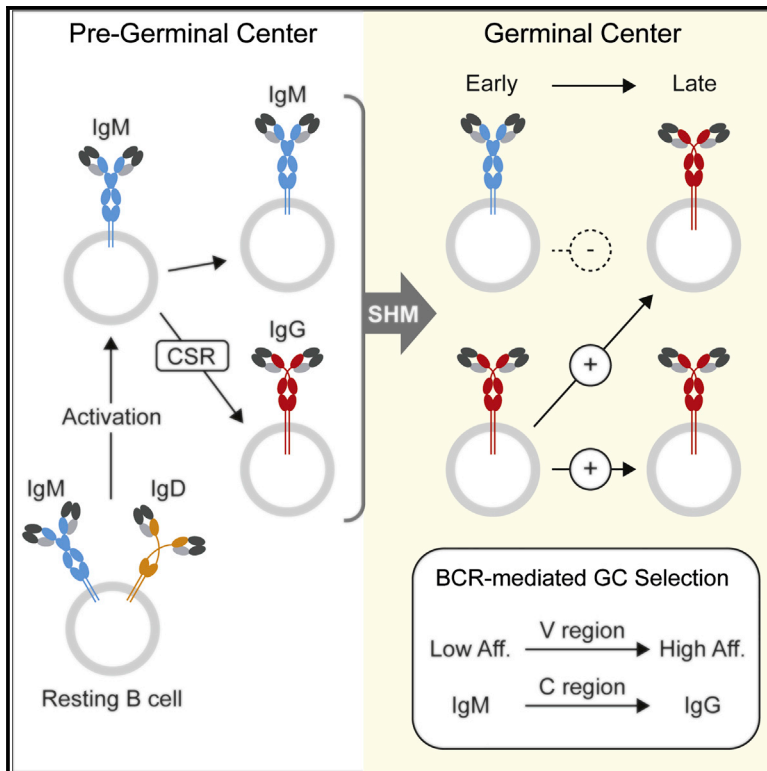


Immunity

Positive selection of IgG⁺ over IgM⁺ B cells in the germinal center reaction

Graphical abstract



Authors

Christopher Sundling,
Angelica W.Y. Lau,
Katherine Bourne, ..., David Zahra,
Dan Suan, Robert Brink

Correspondence

r.brink@garvan.org.au

In brief

Early germinal centers (GCs) contain unswitched IgM⁺ and switched IgG⁺ B cells but ultimately support mature IgG antibody responses. Sundling et al. show that IgG⁺ B cells are enriched and IgM⁺ B cells depleted from GCs by a process of positive selection based on the antigen receptor constant region.

Highlights

- IgM⁺ and IgG⁺ GC B cells both undergo SHM and generate high-affinity variants
- High-affinity IgG⁺ GC B cells are retained over high-affinity IgM⁺ GC B cells
- Positive selection does not require the extended cytoplasmic domain of IgG
- Rare, aberrant IgD⁺ GC B cells are also positively selected over IgM⁺ GC B cells

Article

Positive selection of IgG⁺ over IgM⁺ B cells in the germinal center reaction

Christopher Sundling,^{1,2,3,7} Angelica W.Y. Lau,^{1,4,7} Katherine Bourne,¹ Clara Young,^{1,4} Candy Laurianto,^{1,4} Jana R. Hermes,¹ Rosemary J. Menzies,¹ Danyal Butt,^{1,5} Nike J. Kräutler,^{1,6} David Zahra,^{1,4} Dan Suan,^{1,4} and Robert Brink^{1,4,8,*}

¹Immunology Division, Garvan Institute of Medical Research, Darlinghurst, NSW 2010, Australia

²Division of Infectious Diseases and Center for Molecular Medicine, Department of Medicine Solna, Karolinska Institutet, 17176 Stockholm, Sweden

³Department of Infectious Diseases, Karolinska University Hospital, 17176 Stockholm, Sweden

⁴St. Vincent's Clinical School, UNSW Sydney, Sydney, NSW 2010, Australia

⁵Present address: AbbVie, 100 Research Drive, Worcester, MA 01605, USA

⁶Present address: Neurimmune AG, Wagistrasse 13, 8952 Schlieren-Zurich, Switzerland

⁷These authors contributed equally

⁸Lead contact

*Correspondence: r.brink@garvan.org.au

<https://doi.org/10.1016/j.immuni.2021.03.013>

SUMMARY

Positive selection of high-affinity B cells within germinal centers (GCs) drives affinity maturation of antibody responses. Here, we examined the mechanism underlying the parallel transition from immunoglobulin M (IgM) to IgG. Early GCs contained mostly unswitched IgM⁺ B cells; IgG⁺ B cells subsequently increased in frequency, dominating GC responses 14–21 days after antigen challenge. Somatic hypermutation and generation of high-affinity clones occurred with equal efficiency among IgM⁺ and IgG⁺ GC B cells, and inactivation of Ig class-switch recombination did not prevent depletion of IgM⁺ GC B cells. Instead, high-affinity IgG⁺ GC B cells outcompeted high-affinity IgM⁺ GC B cells via a selective advantage associated with IgG antigen receptor structure but independent of the extended cytoplasmic tail. Thus, two parallel forms of GC B-cell-positive selection, based on antigen receptor variable and constant regions, respectively, operate in tandem to ensure high-affinity IgG antibodies predominate in mature serum antibody responses.

INTRODUCTION

Secreted antibodies confer immune protection by first attaching to foreign antigens through the paired variable regions of their component immunoglobulin (Ig) heavy and light chains—the antibody Fab fragments—and then recruiting destructive effector systems via the heavy chain constant regions (Fc fragment). Depending on heavy chain isotype, antibodies can belong to one of a number of different classes that possess distinct structures and functions. Secreted antibodies of the IgM class (μ heavy chains) are strong activators of complement due to their pentameric structure (Borsos and Rapp, 1965; Sharp et al., 2019) and play an important role in establishing productive antibody responses (Ehrenstein et al., 1998). IgG antibodies (γ heavy chains), on the other hand, are monomeric and can belong to one of four related subclasses (IgG1, IgG2, IgG3, and IgG4 in humans; IgG1, IgG2a/c, IgG2b, and IgG3 in mice). In addition to complement activation, IgG antibodies mobilize a range of cell-based effector mechanisms, including phagocytosis, antibody-dependent cell cytotoxicity, and inflammatory mediator release by engaging with the Fc γ receptors expressed on innate immune effector cells (Nimmerjahn and Ravetch, 2007). Unlike IgM, IgG

antibodies possess an extended, flexible hinge region that allows displacement and rotation of the Fab fragments of the molecule (Huber et al., 1976; Sapphire et al., 2002) and thus promotes high-avidity, bivalent engagement of antigen-bearing targets (Smith et al., 1993; Ye et al., 2016).

Over the course of an immune response, the average affinity of serum antibodies for the initiating antigen progressively increases (antibody affinity maturation; Eisen and Siskind, 1964; Steiner and Eisen, 1967), and there is a transition in antibody class from IgM to IgG (Best et al., 1969; Uhr and Finkelstein, 1963). Thus, early low-affinity IgM antibodies are replaced by more-effective, high-affinity IgG antibodies (Mäkelä et al., 1970). Production of high-affinity IgG is required to achieve effective serological immunity following infection or vaccination (Plotkin et al., 2008). To generate high-affinity IgG, two separate modifications of the Ig genes within responding B cells must occur: (1) somatic hypermutation (SHM) of variable region genes and (2) class-switch recombination (CSR) of constant region genes (Hurwitz et al., 1980; Kim et al., 1981). Both processes rely on the same DNA-modifying enzyme, activation-induced cytidine deaminase (AID) (Feng et al., 2020; Muramatsu et al., 2000).

Activation and differentiation of B cells is controlled by membrane-bound antibodies that comprise the B cell antigen receptor (BCR). Naive B cells initially co-express BCRs of the IgM and IgD classes. Unlike IgM and IgG, IgD is expressed almost exclusively as a BCR rather than secreted antibody and possesses a characteristic, elongated hinge domain (White et al., 1985). Activation by foreign antigen and cognate CD4⁺ T cell help results in downregulation of surface IgD and proliferation of undifferentiated, IgM⁺ B cell blasts. Expression of AID in these early blasts can lead to CSR, whereby the μ heavy chain gene located proximal to the variable region (VDJ) exon is replaced by downstream sequences encoding an alternative heavy chain isotype. In non-mucosal responses, this results in the transition of IgM⁺ into IgG⁺ B cells that will express one of the four γ heavy chain isotypes. BCRs from all IgG subclasses carry an extended 28-amino acid (aa) cytoplasmic domain compared to the short 3-aa tail of IgM, thereby conferring additional response capabilities to switched versus unswitched B cells (Engels et al., 2009; Horikawa et al., 2007; Kaisho et al., 1997; Martin and Goodnow, 2002). The induction of CSR during the early phase of the response is relatively inefficient, and the majority of early B cell blasts remain unswitched (IgM⁺; Roco et al., 2019). Both IgM⁺ and IgG⁺ B cell blasts differentiate into germinal center (GC) B cells around day 5 of the response and migrate into nascent GC structures within the follicles of secondary lymphoid tissues (Chan et al., 2009). Here, they continue to proliferate and express AID but no longer appear to undergo CSR (Roco et al., 2019). Instead, AID activity is directed toward the Ig variable region genes in GC B cells, which undergo intense SHM (Berek et al., 1991; Jacob et al., 1991). GC B cells acquiring BCRs with increased affinity for antigen as a result of SHM are preferentially retained in the GC by a process referred to as positive selection.

High-affinity B cells undergo positive selection in the GC because they are better able to access the foreign antigen displayed in immune complexes on the surface of light zone (LZ)-resident follicular dendritic cells (FDCs) (Victoria and Nussenzweig, 2012). Thus, they are more adept at receiving stimulatory signals in the GC, both directly upon antigen binding and subsequently through presentation of internalized and processed antigen to cognate T follicular helper (Tfh) cells (Victoria et al., 2010). This translates into higher rates of cell cycle activity (Gitlin et al., 2014) and lower rates of apoptosis (Mayer et al., 2017) among high- versus low-affinity GC B cells. High-affinity GC B cells are also more frequently located in the dark zone (DZ), where activated LZ B cells transition to undergo further rounds of SHM and cell division (Gitlin et al., 2014). Mature antibody responses are formed by differentiation of GC B cells into plasma cells. Because plasma cells secrete antibodies that are soluble copies of the BCR, the ongoing SHM and selection of GC B cells expressing high-affinity BCRs forms a clear basis for antibody affinity maturation. On the other hand, the unswitched IgM⁺ GC B cells that dominate early GC responses appear to not undergo CSR and so cannot convert to IgG expression.

Here, we examined the process whereby IgG antibodies come to dominate mature antibody responses. By analyzing the responses of B cells in which the CSR mechanism was specifically compromised, we confirmed that IgM⁺ GC B cells did not undergo CSR and transition into IgG⁺ GC cells. Instead, similar to low-affinity B cells, IgM⁺ B cells were progressively removed

from GCs. This occurred via a form of GC B cell selection determined by the constant region of the BCR rather than its variable region-defined affinity. Thus, unswitched IgM⁺ B cells, despite undergoing normal SHM and generation of high-affinity clones, were depleted from GCs while class-switched IgG⁺ B cells were preferentially retained. The extended cytoplasmic tail present in IgG, but not IgM, BCRs was found not to participate in the positive selection of IgG⁺ GC B cells but impacted negatively upon both antigen receptor expression levels and the expansion of antigen-specific B cells prior to GC formation. Unswitched GC B cells engineered to express IgD instead of IgM did not undergo counter-selection in the GC, suggesting that the activation-induced ablation of IgD expression is required to facilitate preferential retention of switched over unswitched GC B cells. Thus, the two key attributes of serological immunity, increasing antibody affinity and class transition from IgM to IgG, rely on distinct but related forms of positive selection within GCs based on the variable and constant region structures of the BCR, respectively.

RESULTS

IgM⁺ B cells predominate in early GCs but decline in numbers and frequency as the response matures

To investigate changes in Ig heavy chain expression by GC B cells over the course of an immune response, we took advantage of the established SW_{HEL} mouse model in which B cell activation, GC formation, BCR expression, SHM, and affinity maturation can be monitored at high resolution (Brink et al., 2015). B cells from SW_{HEL} mice express BCRs carrying the specificity of the HY-HEL10 monoclonal antibody (mAb) and bind the model protein antigen HEL^{3X} with an affinity of $\sim 10^7$ M⁻¹ (Chan et al., 2012; Paus et al., 2006; Phan et al., 2003). To begin with, small numbers of SW_{HEL} B cells were transferred into wild-type, CD45 congenic, recipient mice and challenged with HEL^{3X} conjugated to sheep red blood cells (HEL^{3X}-SRBC). Class-switching to IgG was evident among antigen-specific (HEL-binding) donor SW_{HEL} B cells in recipient spleens as early as day 2.5 (Figure 1A). At this point, both unswitched (IgM⁺) and switched (IgG⁺) B cells represented undifferentiated CD38^{hi} blasts with high levels of DNA replication (cell cycle activity) as indicated by rapid incorporation of exogenously administered bromodeoxyuridine (BrdU) (Figures 1B and 1C). By day 4.5, the frequency of switched B cells had increased ~ 4 -fold (Figure 1A), with cell cycle activity at this point restricted to the IgM⁺ and IgG⁺ B cells that had undergone differentiation into CD38^{lo} GC B cells (Figures 1B and 1C).

The limited CSR that occurred during the initial phase of the response resulted in early (day 4.5) GCs made up predominantly of unswitched GC B cells, with IgM⁺ outnumbering IgG⁺ GC B cells by a factor of 2:1 (Figures 1D and 1E). This ratio remained unchanged over the next 2 days (Figures 1D and 1E), consistent with cessation of CSR upon GC B cell differentiation (Roco et al., 2019). Over the subsequent 7 days, however, the frequency of IgG⁺ GC B cells increased so that, by day 13.5, they outnumbered IgM⁺ GC B cells by a factor of greater than 7:1 (Figures 1D and 1E). When total numbers of switched and unswitched GC B cells were compared, it was apparent that the major reason for the progressive increase in frequency of IgG⁺ B cells was a steep decrease in the numbers of IgM⁺ GC B cells between days 6.5 and 13.5 (Figure 1F). Analysis of serum

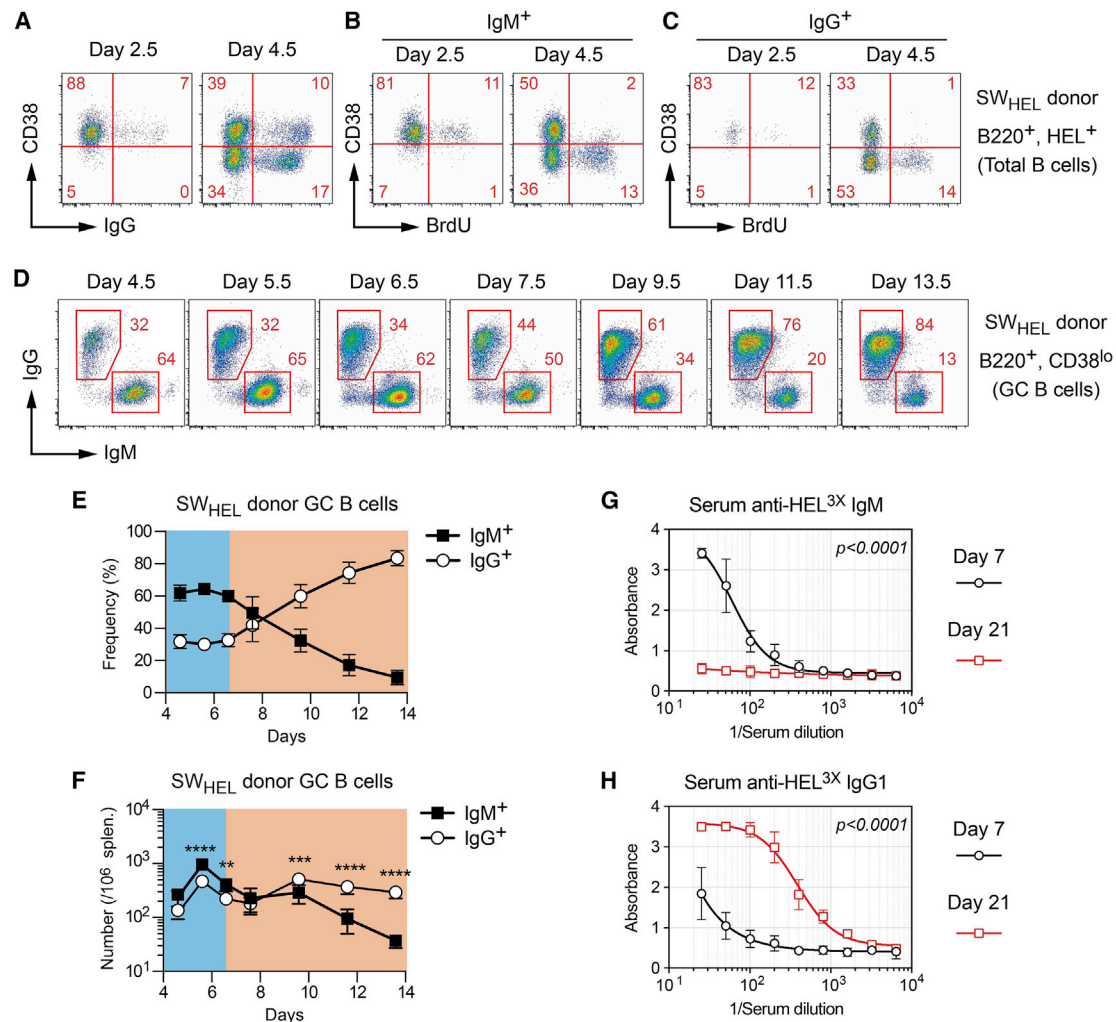


Figure 1. IgM⁺ B cells predominate in early GCs but decline in numbers and frequency as the response matures

(A) Representative flow cytometry plots showing frequency of donor-derived, HEL-specific, IgG-switched B cell blasts (CD38^{hi}, IgG⁺) and GC B cells (CD38^{lo}, IgG⁺) 2.5 and 4.5 days after SW_{HEL} B cells transfer and challenge with HEL^{3X}-SRBC.

(B and C) Representative flow cytometry plots showing BrdU incorporation into IgM⁺ (B) and IgG⁺ (C) HEL-specific B cell blasts and GC B cells 2.5 and 4.5 days after transfer and challenge and 1 h after BrdU administration intravenously (i.v.).

(D) Representative flow cytometry plots showing frequency of SW_{HEL} donor-derived unswitched (IgM⁺) and class-switched (IgG⁺) GC B cells from days 4.5 to 13.5 after transfer and challenge.

(E and F) Frequency within donor-derived GC responses (E) and number per 10⁶ splenocytes (F) of IgM⁺ and IgG⁺ donor-derived GC B cells over time as for (D). Blue and orange areas indicate the time periods before and after the beginning of the transition from predominance of IgM⁺ to IgG⁺ GC B cells at day 6.5.

(G and H) ELISA of HEL^{3X}-binding serum IgM (G) and IgG1 (H) antibodies in recipient mice on days 7 and 21.

Data in (A)–(F) are representative of 3 to 4 experiments. Data in (E) and (F) correspond to mean ± SD with 5 mice per group. Statistics was calculated using two-way ANOVA with Bonferroni's post-test. Data in (G) and (H) correspond to mean ± SD from 5 mice per group representing two independent experiments. **p < 0.01; ***p < 0.001; ****p < 0.0001.

antibodies directed against HEL^{3X} early (day 7) and late (day 21) in the response confirmed that the observed shift from IgM to IgG BCR expression by GC B cells was associated with the normal transition from IgM to IgG serum antibodies as the response matured (Figures 1G and 1H).

The decline of the IgM⁺ GC B cell population is not due to ongoing CSR

Although CSR appears to be infrequent among GC B cells (Roco et al., 2019), the most straightforward explanation for our results

was that IgM⁺ B cells were progressively converted into IgG⁺ B cells by ongoing CSR within the GC. To test this possibility, we tested whether IgM⁺ GC B cells with absent or greatly reduced CSR capabilities were still depleted over the course of the GC response. In the first instance, we utilized an additional Ig-transgenic mouse strain (MD4) in which B cells express the same Hy-HEL10 specificity as SW_{HEL} B cells but cannot undergo CSR (Goodnow et al., 1988). Naive SW_{HEL} and MD4 B cells (distinguishable by CD45 allotype; Figures S1A and S1B) were co-transferred into wild-type recipient mice and challenged with

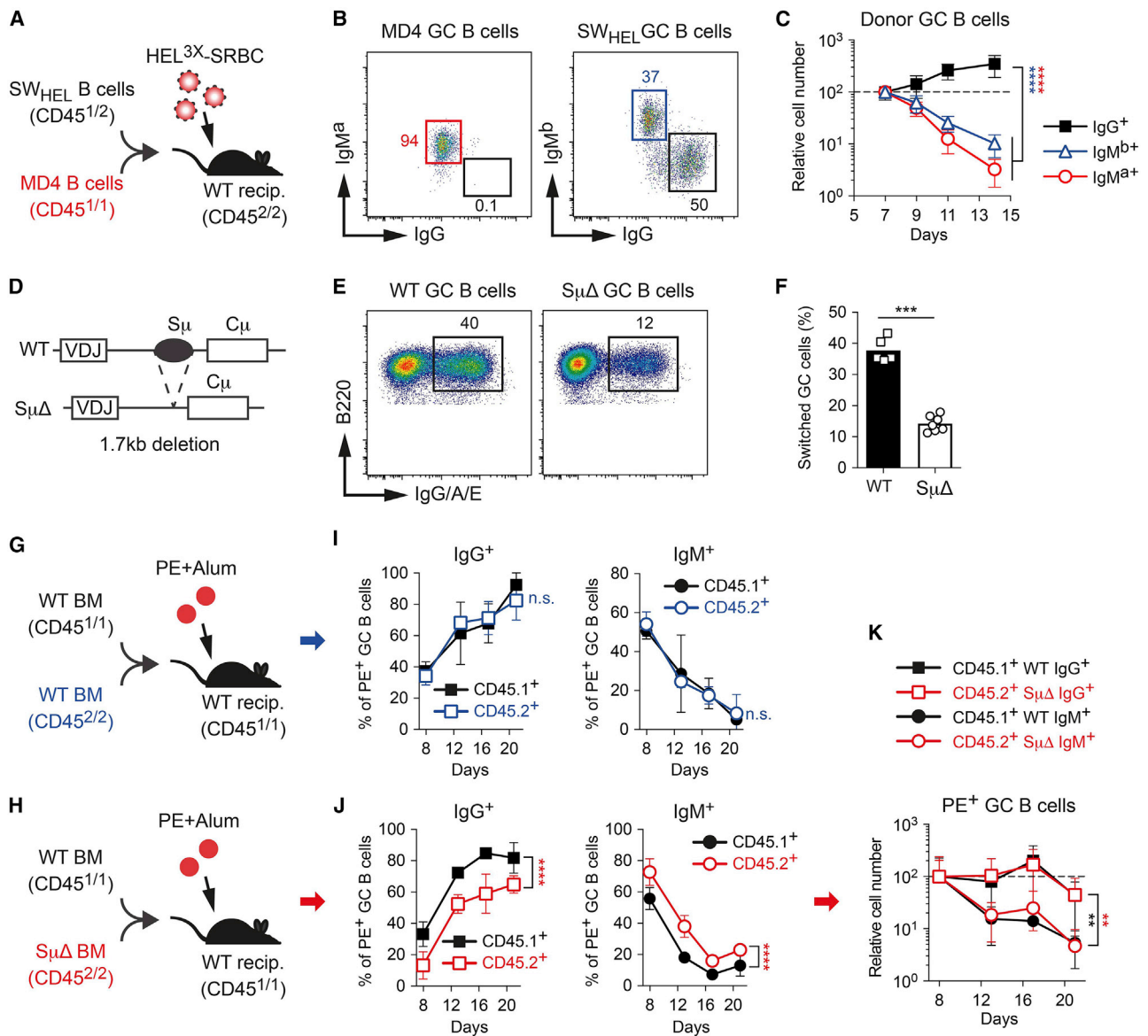


Figure 2. The decline of the IgM⁺ GC B cell population is not due to ongoing CSR

(A) Schematic of co-transfer experiment: spleen cells from SW_{HEL} (CD45^{1/2}) and MD4 (CD45^{1/1}) donor mice (1 × 10⁴ and 2 × 10⁴ HEL-binding B cells, respectively) were co-transferred into CD45^{2/2} recipients, challenged with HEL^{3X}-SRBC, and responses in recipient spleens analyzed from 7 to 14 days later.

(B) Representative flow cytometry plots of IgM versus IgG expression (day 9) on GC B cells derived from MD4 (CD45.1⁺ and CD45.2⁺) and SW_{HEL} (CD45.1⁺ and CD45.2⁺) donors (MD4 expresses IgM^a; SW_{HEL} expresses IgM^b).

(C) Kinetics of unswitched MD4 (IgM^{a+}) and SW_{HEL} (IgM^{b+}) GC B cells and class-switched SW_{HEL} (IgG⁺) GC B cells. Data show mean ± SD normalized to day 7 cell numbers. Overall IgM^{a+} and IgM^{b+} GC B cell numbers were compared to IgG⁺ GC B cells by two-way ANOVA followed by Bonferroni's post-test. ****p < 0.0001. Data are representative of two independent experiments.

(D) Schematic of the μ switch-region deletion in the Ig heavy chain locus of the SμΔ mouse (see Figure S1E).

(E) Representative flow cytometry plots showing frequency of class-switched (IgG⁺/IgA⁺/IgE⁺) B cells within GCs present in wild-type and SμΔ mice 10 days post-SRBC challenge.

(F) Frequency of class-switched (IgG⁺/IgA⁺/IgE⁺) B cells within GCs present in wild-type (n = 5) and SμΔ (n = 7) mice 10 days post-SRBC challenge. Bar graphs show mean ± SEM. Statistics were evaluated using an unpaired Student's t test with ***p < 0.001. Data are representative of two experiments.

(G and H) Schematic of mixed bone marrow chimera experiments: wild-type CD45^{1/1} recipient mice were lethally irradiated and rescued with 50:50 mixes of bone marrow cells from wild-type CD45^{1/1} and wild-type CD45^{2/2} mice (G) or wild-type CD45^{1/1} and SμΔ CD45^{2/2} mice (H). Following reconstitution, chimeras were challenged intraperitoneally (i.p.) with PE in alum.

(I) Frequency of IgG⁺ and IgM⁺ cells among PE-specific GC B cells derived from wild-type (CD45.1⁺) and wild-type (CD45.2⁺) donor B cells.

(legend continued on next page)

HEL^{3X}-SRBC (Figure 2A). Donor-derived GC responses contained a mixture of IgM⁺ MD4 (IgM^a allotype), IgM⁺ SW_{HEL} (IgM^b allotype), and IgG⁺ SW_{HEL} GC B cells (Figure 2B). Each of these populations underwent SHM and affinity maturation as revealed by the increasing frequency of cells capable of binding low concentrations of HEL^{3X} antigen over the course of the response (Figures S1C and S1D; Chan et al., 2012; Phan et al., 2006). Analysis of the GC responses of these co-transferred B cells revealed that the numbers of donor-derived IgG⁺ GC B cells increased from day 7 onward. By contrast, the numbers of both MD4-derived and SW_{HEL}-derived IgM⁺ GC B cells declined rapidly and with similar kinetics (Figure 2C). In this system, therefore, the depletion of IgM⁺ B cells from the GC response could not be explained by CSR-mediated conversion into IgG⁺ B cells.

To determine whether the same result would be obtained in polyclonal GC responses formed from the natural primary repertoire, we used CRISPR-Cas9-mediated gene targeting to generate a line of mutant mice S_μΔ in which CSR is compromised through removal of the switch-recombination sequences 5' of the μ heavy chain constant region gene (Figures 2D and S1E). To verify that CSR was reduced as a result of this deletion, S_μΔ and control wild-type mice were challenged with unconjugated SRBCs. Analysis of splenic GC B cell responses on day 10 after challenge showed that switching events were reduced by ~3-fold in S_μΔ mice (Figures 2E and 2F), consistent with observations made in a similar S_μ mutant line (Khamilichi et al., 2004).

Next, chimeric mice were produced by rescuing lethally irradiated recipients with a 50:50 mix of bone marrow from wild-type CD45.1⁺ donors and either wild-type (Figure 2G) or S_μΔ (Figure 2H) CD45.2⁺ donors. In this case, chimeras were immunized with phycoerythrin (PE) and the splenic GC responses of PE-binding B cells monitored by flow cytometry (Pape et al., 2011). Similar to our observations after SRBC challenge, the proportion of PE-specific GC B cells that switched to IgG was ~3-fold lower in S_μΔ compared to wild-type B cells on day 8 of the response (Figures 2I and 2J). Analysis of anti-PE GC responses in control chimeras revealed increasing IgG⁺ and decreasing IgM⁺ GC B cell frequencies over the course of the response (Figure 2I), similar to our observations in the SW_{HEL} donor system (Figure 1E). Despite the relatively low frequencies of IgG⁺ B cells on day 8 of S_μΔ-derived GC responses, these also increased at the expense of IgM⁺ GC B cells as the response to PE progressed (Figure 2J). After normalizing cell numbers to compensate for the different composition of the wild-type and S_μΔ GC responses on day 8, it was apparent that IgM⁺ GC B cells decreased in numbers with the same kinetics, regardless of whether or not they carried the S_μΔ deletion (Figure 2K). These results clearly demonstrated that both SW_{HEL} donor and endogenous anti-PE GC responses were characterized by the progressive enrichment of IgG⁺ B cells at the expense of IgM⁺ B cells. Importantly, these results also established that the transition to a predominance of IgG⁺ B cells within the GC occurred independently of CSR in each case.

IgM⁺ GC B cells do not preferentially differentiate into MBCs or PCs

In the absence of CSR-mediated transition to IgG expression, the declining frequency of IgM⁺ B cells over the course of the GC response must instead proceed via preferential retention of IgG⁺ B cells within the GC. Because B cells exit the GC when they differentiate into memory B cells (MBCs) or plasma cells (PCs), one possible explanation was that IgM⁺ GC B cells progress more frequently along one or both of these differentiation pathways. To test this, we compared the frequencies of MBC and PC precursors among IgM⁺ and IgG⁺ GC B cells on day 9 of the response of SW_{HEL} B cells to HEL^{3X}-SRBC.

MBC precursors originate in the LZ of the GC and are identifiable through their expression of chemokine receptor CCR6 (i.e., CD86^{hi}, CXCR4^{lo}, and CCR6⁺; Suan et al., 2017). In agreement with previous results (Suan et al., 2017), MBC precursors were found to be greatly enriched among LZ B cells that still retained low affinity for the antigen (Figures 3A and 3B). When the CCR6⁻ and CCR6⁺ subsets of the low-affinity LZ compartment were compared, similar proportions of IgM⁺ and IgG⁺ were found in each case (Figure 3A). Moreover, the proportions of CCR6⁺ MBC precursors among low-affinity IgM⁺ and IgG⁺ LZ B cells did not differ significantly (Figure 3B), indicating that there was no detectable difference in the propensity of IgM⁺ and IgG⁺ GC B cells to undergo MBC differentiation.

PC precursors also reside in the LZ of the GC, where they can be identified by the expression of a Blimp1-GFP reporter gene (Kallies et al., 2004). Unlike MBC precursors, however, PC precursors are enriched within the high-affinity compartment of the LZ (Kräutler et al., 2017). Analysis of the GC response derived from SW_{HEL} B cells carrying the Blimp1-GFP reporter gene revealed that the Blimp1-GFP⁺ PC precursor subset within the high-affinity LZ B cell compartment contained a greater proportion of IgG⁺ B cells (and therefore a lower proportion of IgM⁺ B cells) than the Blimp1-GFP⁻ subset (Figure 3C). Additionally, Blimp1-GFP⁺ PC precursors were less rather than more frequent among IgM⁺ compared to IgG⁺ B cells within the high-affinity LZ compartment (Figure 3D). Taken together, these data showed that the declining frequency of IgM⁺ GC B cells over the course of the response could not be attributed to them undergoing higher levels of MBC or PC differentiation than IgG⁺ GC B cells. Instead, it appeared that IgG⁺ GC B cells show a greater propensity to undergo PC differentiation compared to IgM⁺ GC B cells.

IgM⁺ GC B cells undergo normal SHM and production of high-affinity clones

Another possible explanation for the failure of IgM⁺ B cells to persist in the GC was that they undergo SHM at a slower pace and/or generate fewer high-affinity clones than IgG⁺ GC B cells. To test this possibility, SW_{HEL} B cells were challenged with HEL^{3X}-SRBC and the IgG⁺ and IgM⁺ compartments of the GC response monitored for affinity maturation and SHM. High-affinity GC B cells revealed by flow cytometric staining with a low concentration of soluble HEL^{3X} antigen (50 ng/mL) have acquired the

(J) Frequency of IgG⁺ and IgM⁺ cells among PE-specific GC B cells derived from wild-type (CD45.1⁺) and S_μΔ (CD45.2⁺) donor B cells. Statistics were evaluated using two-way ANOVA followed by Bonferroni post hoc test. *p < 0.05; **p < 0.01; ***p < 0.001; ****p < 0.0001.

(K) Relative numbers of IgG⁺ and IgM⁺ PE-specific GC B cells derived from wild-type (CD45.1⁺) and S_μΔ (CD45.2⁺) donor B cells. Data were normalized to the number of each subset present on day 8. Data show mean ± SD and represent 4 to 5 mice unless stated otherwise.

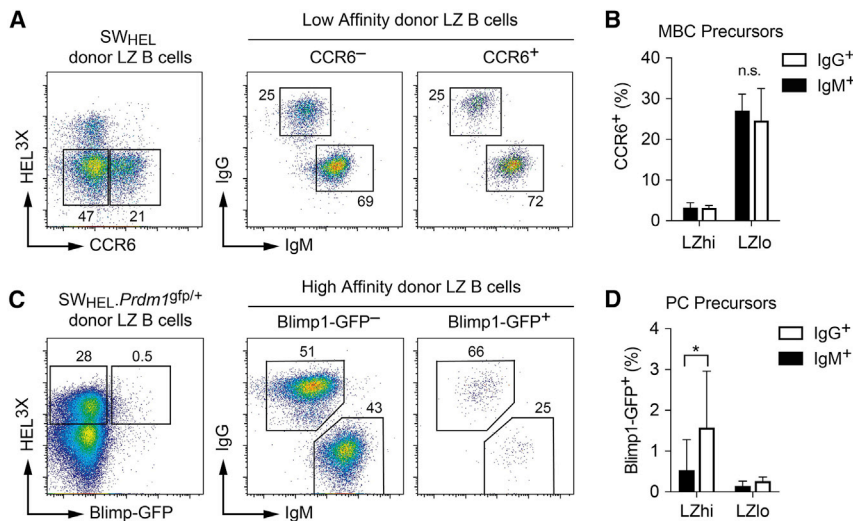


Figure 3. IgM⁺ GC B cells do not preferentially differentiate into MBCs or PCs

SW_{HEL} (A and B) or SW_{HEL}.Blimp1^{9fp/+} (C and D) donor B cells were transferred and challenged with HEL^{3X}-SRBC in wild-type recipients. Representative flow cytometry plots show donor-derived GC LZ cells (CXCR4^{lo}, CD86^{hi}) on day 8 (A and B) or day 9 (C and D) with high- and low-affinity cells resolved by staining with 50 ng/mL HEL^{3X} (A and C). (A) Expression of IgM and IgG in the CCR6⁺ and CCR6⁻ low-affinity GC LZ compartments. (B) Frequency of IgM⁺ and IgG⁺ MBC precursors (CCR6⁺) in high-affinity and low-affinity GC LZ compartments. (C) Expression of IgM and IgG in Blimp1-GFP⁺ and Blimp1-GFP⁻ high-affinity GC LZ compartments. (D) Frequency of IgM⁺ and IgG⁺ PC precursors (Blimp1-GFP⁺) in high- and low-affinity GC LZ compartments. Data in (B) and (D) show mean ± SD with 5–10 mice per group. Data are representative of 2 to 3 experiments. Statistics were evaluated using two-way ANOVA with Bonferroni's post hoc test. *p < 0.05.

canonical Y53D substitution in their heavy chain variable region gene and obtained an ~100-fold increased affinity for HEL^{3X} (Chan et al., 2012; Phan et al., 2006). These high-affinity cells were detectable on day 7 of the response at a frequency of ~5% among both IgM⁺ and IgG⁺ GC B cells (Figure 4A). Strikingly, high-affinity IgG⁺ B cells subsequently accumulated in the GC, whereas high-affinity IgM⁺ GC B cells did not (Figures 4A and 4B). Accordingly, SHM analysis revealed that the incidence of the high-affinity Y53D substitution was significantly greater among IgG⁺ compared to IgM⁺ GC B cells on day 9 of the response (Figure 4C). Nevertheless, IgM⁺ and IgG⁺ GC B cells had undergone SHM at equivalent rates (Figure 4D), demonstrating that IgM⁺ GC B cells were not impaired in their capacity to undergo SHM. Instead, it was apparent that high-affinity IgM⁺ B cells carrying the Y53D substitution were efficiently generated but failed to accumulate in the GC, whereas high-affinity IgG⁺ B cells with the same antigen affinity were selectively retained.

IgG⁺ GC B cells are positively selected at the expense of IgM⁺ GC B cells

The selective retention of IgG⁺ over IgM⁺ B cells in the GC has strong parallels with the positive selection of high-affinity over low-affinity GC B cells. In particular, both processes appear to operate by retaining defined subsets of GC B cells based on specific properties of their BCR. We speculated, therefore, that the fundamental mechanisms that drive positive selection of high-affinity GC B cells may also be responsible for selective retention of IgG⁺ B cells in the GC. To investigate this possibility, we next tested whether the features that characterize positive selection of high- versus low-affinity GC B cells are shared by IgG⁺ versus IgM⁺ GC B cells.

First, positively selected GC B cells transit more frequently from LZ to DZ, with the result that high-affinity GC B cells have a greater representation in the DZ compartment (CD86^{lo} and CXCR4^{hi}) than low-affinity GC B cells (Gitlin et al., 2014). This phenomenon was already evident in our system on day 7 of the SW_{HEL} B cell response to HEL^{3X}-SRBC, with both high-affinity IgM⁺ and IgG⁺ GC B cells being more prevalent in the DZ than

their low-affinity counterparts (Figure 4E). Among the high-affinity GC B cells present on day 7, it was also apparent that the IgG⁺ subset contained a higher proportion of DZ phenotype cells compared to IgM⁺ cells (Figure 4E). Moreover, from this time point onward, IgG⁺ GC B cells consistently showed greater representation in the DZ than IgM⁺ GC B cells (Figures 4F and 4G). Significantly, the day 7 time point at which preferential localization of IgG⁺ GC B cells to the DZ first becomes evident (Figure 4G) corresponds with the point at which selective retention of IgG⁺ B cells in the GC commences (Figure 1E).

Another feature of positively selected, high-affinity GC B cells is that they are more frequently in active cell cycle than low-affinity GC B cells (Gitlin et al., 2014). This phenomenon was also evident on day 7 of the SW_{HEL} B cell response to HEL^{3X}-SRBC, with both the high-affinity IgM⁺ and IgG⁺ LZ B cell compartments containing 3- to 4-fold higher frequencies of cells undergoing active DNA replication (BrdU incorporation) compared to their low-affinity counterparts (Figure 4H). This was still the case on day 10 of the response (Figure 4I). By this time point, however, it was also evident that a significantly greater proportion of high-affinity IgG⁺ LZ B cells was actively cycling compared to high-affinity IgM⁺ LZ B cells (Figures 4I, S2A, and S2B). Although lower rates of apoptosis among high- versus low-affinity GC B cells were observed upon intracellular staining for active caspase-3 (Mayer et al., 2017), we did not detect a significant difference in apoptosis rates between IgM⁺ and IgG⁺ GC B cells (Figures S2C and S2D). Nevertheless, taken together, these data are consistent with the hypothesis that the selective retention of IgG⁺ over IgM⁺ GC B cells is achieved by employing similar fundamental mechanisms to those that selectively retain high-affinity B cells in the GC. It appears, therefore, that GC B cells can undergo positive selection based on the heavy chain constant region of their BCR in addition to their variable region-defined affinity for antigen.

Positive selection of IgG1⁺ GC B cells is not mediated by the IgG1 cytoplasmic tail

We next sought to determine what feature(s) of IgG⁺ GC B cells facilitated their positive selection in the GC. One possibility was

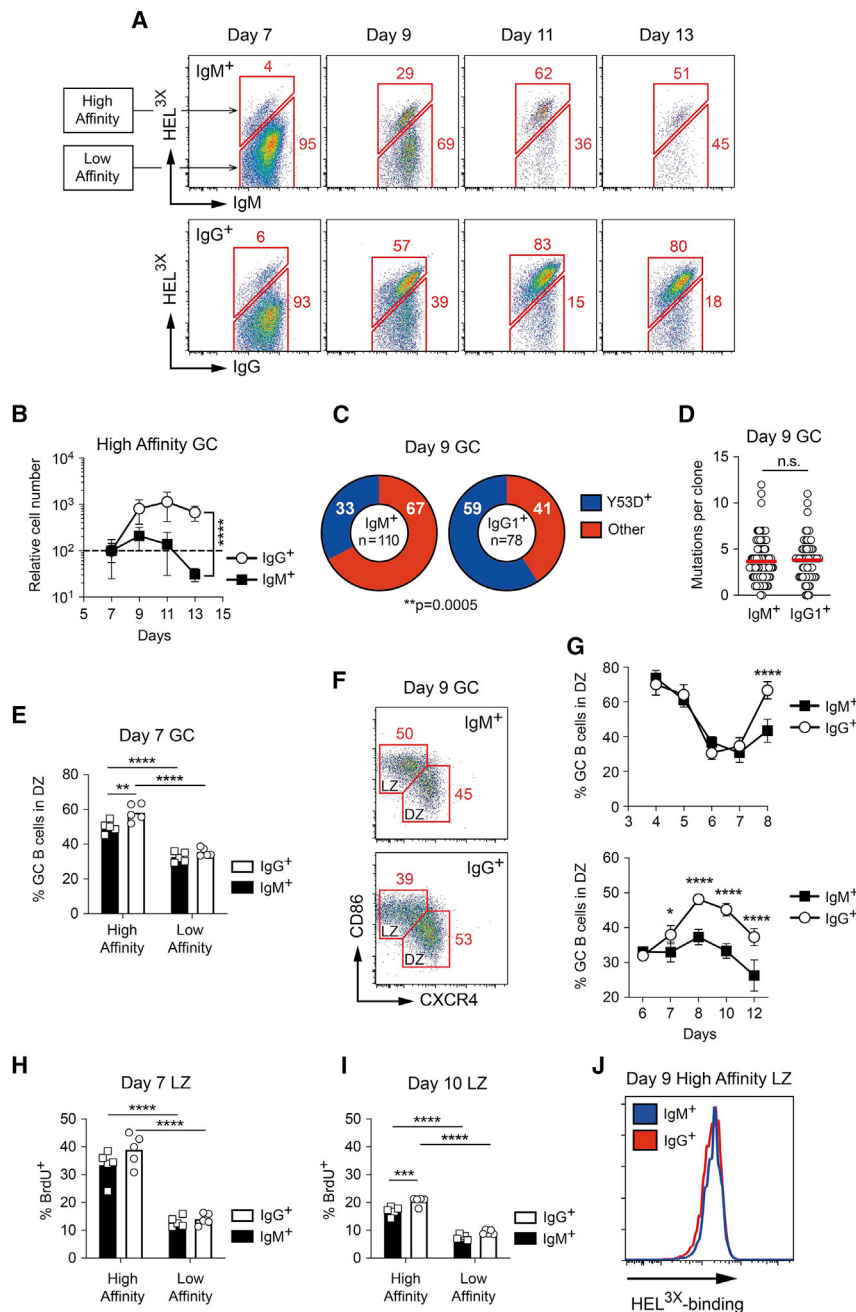


Figure 4. IgG⁺ GC B cells are positively selected at the expense of IgM⁺ GC B cells

(A) Representative flow cytometry plots showing SW_{HEL} donor-derived IgM⁺ and IgG⁺ GC B cells in spleens of wild-type recipients following transfer and challenge with HEL^{3X}-SRBC. Cells with high affinity for HEL^{3X} were identified by staining with 50 ng/mL HEL^{3X}.

(B) Time course analysis of the numbers of high-affinity IgG⁺ and IgM⁺ GC B cells normalized to day 7.

(C and D) Single, SW_{HEL} donor-derived IgM⁺ and IgG⁺ GC B cells were sorted for SHM analysis of the Ig heavy chain variable region gene on day 9. Data are pooled from two experiments. Statistics were evaluated using Fisher's exact test.

(C) Pie charts indicate frequencies of somatically mutated clones with or without the high-affinity Y53D substitution. n, number of clones analyzed.

(D) Graph indicates the number of somatic mutations identified in the Ig variable region exon of each IgM⁺ and IgG⁺ GC B cell clone. Means are indicated by red lines.

(E) Frequencies of high- versus low-affinity IgM⁺ and IgG⁺ SW_{HEL} GC B cells with a DZ (CXCR4^{hi}, CD86^{lo}) phenotype on day 7.

(F) Representative flow cytometry plots showing LZ (CXCR4^{lo}, CD86^{hi}) versus DZ (CXCR4^{hi}, CD86^{lo}) compartmentalization of SW_{HEL} donor-derived IgM⁺ and IgG⁺ GC B cells on day 9.

(G) Time course of the proportion of SW_{HEL} donor-derived IgM⁺ and IgG⁺ GC B cells with a DZ phenotype during early (top) and later (bottom) phases of response.

(H and I) Frequency of high- versus low-affinity IgM⁺ and IgG⁺ SW_{HEL} LZ B cells staining for BrdU 7 days (H) and 10 days (I) after transfer and challenge and 1 h after BrdU administration i.v.

(J) Histogram showing equivalent levels of antigen (HEL^{3X}) binding on high-affinity IgM⁺ and IgG⁺ LZ B cells on day 9.

Data in (B), (E), (G), (H), and (I) show mean ± individual mice or SD of 5 mice per time point per group. Statistics were evaluated using two-way ANOVA followed by Bonferroni's post hoc test. **p < 0.01, ***p < 0.001, and ****p < 0.0001, unless stated otherwise.

that IgG BCRs are expressed at higher surface densities than IgM BCRs, thus facilitating greater access to antigen and delivery of stimulatory signals to IgG⁺ over IgM⁺ GC B cells. This was not the case, however, because high-affinity IgG⁺ and IgM⁺ LZ B cells were found to bind equivalent levels of HEL^{3X} antigen over the course of the GC response (Figures 4J and S2E). Instead, we postulated that differences in the structure of γ and μ membrane heavy chains provide the basis for positive selection of IgG⁺ over IgM⁺ GC B cells.

The extended cytoplasmic tail carried by IgG, but not IgM, BCRs has been proposed to augment intracellular calcium mobilization and increase the proliferative expansion of B cell blasts in

tested whether the extended cytoplasmic domain of IgG is responsible for the preferential retention of IgG⁺ over IgM⁺ GC B cells. To facilitate these studies, CRISPR-Cas9-mediated gene targeting was used to produce a series of genetically modified (GM) SW_{HEL} mouse lines that carried specific alterations to the constant region sequences of the Ig heavy chain gene into which the HyHEL10 variable region gene had previously been incorporated.

First, the SW_{HEL}.IgG1cyt Δ mouse line was produced in which class-switched, IgG1⁺ SW_{HEL} B cells express a truncated form of IgG1 lacking the extended cytoplasmic domain. A single base change was introduced into the SW_{HEL} γ 1 heavy chain locus to

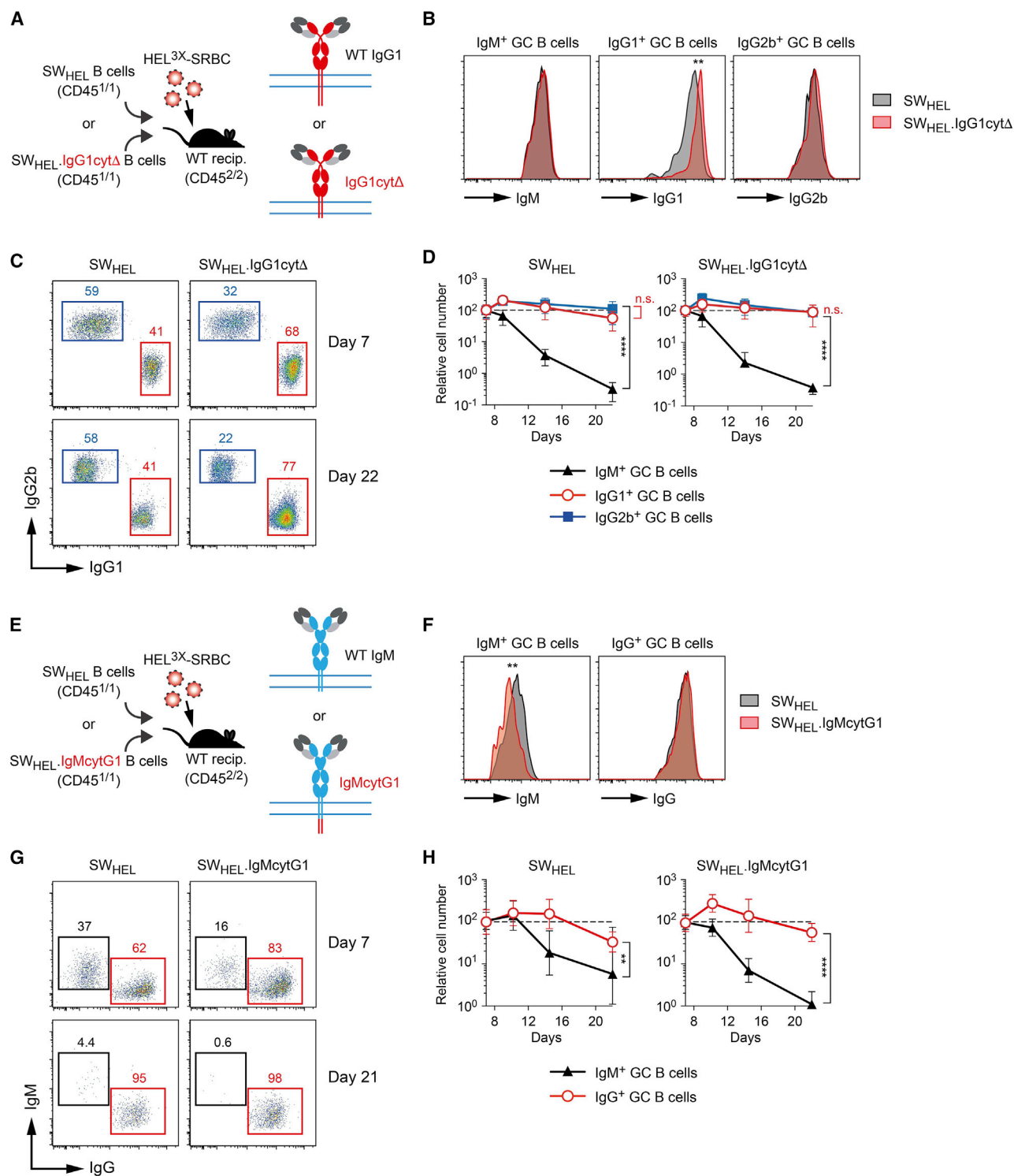


Figure 5. Positive selection of IgG⁺ GC B cells is not mediated by the IgG1 cytoplasmic tail

(A) Schematic of transfer experiment: wild-type SW_{HEL} or SW_{HEL}.IgG1cytΔ B cells (both CD45^{1/1}) were transferred into CD45^{2/2} wild-type recipients, challenged with HEL^{3X}-SRBC, and recipients analyzed from days 7 to 22.

(B) Histogram overlays indicating BCR expression levels on SW_{HEL} versus SW_{HEL}.IgG1cytΔ donor-derived IgM⁺, IgG1⁺, and IgG2b⁺ GC B cells on day 10. p values were calculated based on mean fluorescence intensities (MFIs) from 5 replicate mice using an unpaired Student's t test. **p < 0.01. Data are representative of two experiments.

form a premature stop codon that truncated the cytoplasmic domain of membrane IgG1 such that it was identical to the 3-aa tail of IgM (Figures S3A and S3B). To assess the impact of this mutation on IgG1-switched GC B cells, B cells from SW_{HEL} and SW_{HEL}.IgG1cytΔ mice were transferred separately into wild-type recipient mice (Figure 5A) and their responses to HEL^{3X}-SRBC compared. Surprisingly, IgG1⁺ GC B cells derived from SW_{HEL}.IgG1cytΔ donor cells were found to express significantly higher levels of BCR than those derived from wild-type SW_{HEL} donors (Figure 5B). This effect was specific for IgG1, because BCR levels on IgM⁺ and IgG2b⁺ GC B cells were unaffected (Figure 5B). IgG1⁺ GC B cells derived from SW_{HEL}.IgG1cytΔ donors also made a significantly larger contribution to the early (day 7) GC response than those from wild-type SW_{HEL} mice (Figures 5C and S3C), whereas the contributions of IgM⁺ and IgG2b⁺ B cells did not differ (Figure S3C). Nonetheless, from day 7 of the GC response onward, the relative numbers of IgG1⁺ and IgG2b⁺ GC B cells derived from each donor genotype followed a similar stable trajectory, with IgM⁺ GC B cells declining rapidly as expected in each case (Figure 5D). Thus, despite the impact upon early responses and BCR expression levels, the removal of the cytoplasmic domain from IgG1 had no detectable impact upon the retention of IgG1⁺ B cells in the GC.

To further investigate the functional capabilities of the IgG1 cytoplasmic tail, we next produced the SW_{HEL}.IgMcytG1 mouse line in which IgM was modified to carry an extended cytoplasmic domain identical to that of IgG1. In this case, sequence encoding the 25-aa extension specific to the membrane γ 1 heavy chain was inserted immediately prior to the stop codon of the SW_{HEL} μ membrane heavy chain gene (Figures S3B and S3D). Consistent with the impact of removing these sequences from IgG1 BCRs, addition of the IgG1 tail resulted in lower membrane IgM expression on naïve B cells and reduced overall antigen binding capacity (Figure S3E). To test whether addition of the IgG1 cytoplasmic tail to IgM might nevertheless improve the retention of unswitched B cells in the GC, naïve B cells from SW_{HEL} and SW_{HEL}.IgMcytG1 mice were transferred separately into wild-type recipient mice (Figure 5E) and their responses to HEL^{3X}-SRBC compared. As observed on naïve B cells, IgM⁺ GC B cells derived from SW_{HEL}.IgMcytG1 donor cells expressed a lower BCR density than those derived from SW_{HEL} controls (Figure 5F). In addition, the numbers of IgM⁺, but not IgG⁺, B cells present in day 7 GCs were reduced in SW_{HEL}.IgMcytG1 B cell responses (Figures 5G and S3F). Subsequent tracking of the retention of

switched and unswitched B cells over the course of the GC response revealed that IgM⁺ B cells were efficiently depleted from the GC with or without the addition of the IgG1 cytoplasmic tail (Figure 5H). Taken together, these data show that the presence of the IgG1 cytoplasmic tail in either IgM or its native IgG1 BCR reduces antigen receptor expression and limits B cell expansion prior to GC formation. In both cases, however, the presence of the IgG1 cytoplasmic tail provided no apparent selective advantage within the GC, indicating that some other difference between IgG and IgM BCRs is likely responsible for the selective retention of IgG⁺ B cells in the GC.

Expression of IgD instead of IgM prevents counter-selection of unswitched GC B cells

Although a difference in structure/function between IgG and IgM BCRs is the most obvious explanation for the retention of switched over unswitched B cells in the GC, it was also possible that the process of CSR itself may in some way alter the responsiveness of GC B cells to give them an intrinsic selective advantage over unswitched GC B cells. If so, we reasoned that B cells that had not undergone class switching but expressed BCR other than IgM should still be depleted over the course the GC response.

To create such a scenario, a third line of GM SW_{HEL} mice was produced (SW_{HEL}.IgMΔ), in which the μ heavy chain constant region sequences were deleted and the δ heavy chain constant region gene thereby moved proximal to the HyHEL10 variable region exon (Figure S4A). As observed in mice carrying a similarly arranged immunoglobulin transgene (Brink et al., 1992), IgD was expressed instead of IgM during B cell development in SW_{HEL}.IgMΔ mice, and mature HEL-binding B cells expressed IgD only instead of co-expressing IgM and IgD (Figure S4B). Analysis of parallel GC responses from SW_{HEL}.IgMΔ and wild-type SW_{HEL} B cells (Figure 6A) revealed that both responses generated similar numbers of class-switched IgG⁺ GC B cells (Figures 6B and 6C). However, the numbers of unswitched IgD⁺ GC B cells derived from SW_{HEL}.IgMΔ donor B cells was almost 10-fold greater than the numbers of unswitched IgM⁺ GC B cells from wild-type SW_{HEL} donor B cells (Figures 6B and 6C). This appears to be due to a greater expansion of IgD⁺ B cells prior to GC formation, potentially ascribable to their higher initial BCR density (Figure S4B) or to the ability of IgD BCRs to enhance early proliferative responses. Once within the GC, IgD⁺ B cells expressed slightly lower surface BCR densities (HEL^{3X}-binding) than IgM⁺ and IgG⁺ B cells (Figure S4C) but nevertheless underwent efficient affinity maturation to HEL^{3X} (Figure 6D).

(C) Representative flow cytometry plots showing the contributions of IgG1⁺ and IgG2b⁺ B cells to GC responses derived from SW_{HEL} and SW_{HEL}.IgG1cytΔ donor B cells. Data from GC B cells not expressing IgG1 or IgG2b are omitted.

(D) Kinetics of IgM⁺, IgG1⁺, and IgG2b⁺ GC B cell responses derived from SW_{HEL} and SW_{HEL}.IgG1cytΔ donor B cells, expressed relative to day 7. Statistics were calculated using two-way ANOVA followed by Bonferroni's post hoc test. ****p < 0.0001.

(E) Schematic of transfer experiment: wild-type SW_{HEL} or SW_{HEL}.IgMcytG1 B cells (both CD45^{1/1}) were transferred into CD45^{2/2} wild-type recipients, challenged with HEL^{3X}-SRBC, and recipients analyzed from days 7 to 21.

(F) Histogram overlays indicating BCR expression levels on SW_{HEL} versus SW_{HEL}.IgMcytG1 donor-derived IgM⁺ and IgG⁺ GC B cells on day 10. p values were calculated based on MFIs from 5 replicate mice using unpaired Student's t test. **p < 0.01.

(G) Representative flow cytometry plots showing the contributions of IgM⁺ and IgG⁺ B cells to GC responses derived from SW_{HEL} and SW_{HEL}.IgMcytG1 donor B cells. Data from GC B cells not expressing IgM or IgG are omitted.

(H) Kinetics of IgM⁺ and IgG⁺ GC B cell responses derived from SW_{HEL} and SW_{HEL}.IgMcytG1 donor B cells, expressed relative to day 7. Statistics were calculated using two-way ANOVA followed by Bonferroni's post hoc test. **p < 0.01; ****p < 0.0001.

Data in (C) and (D) are representative of two experiments.

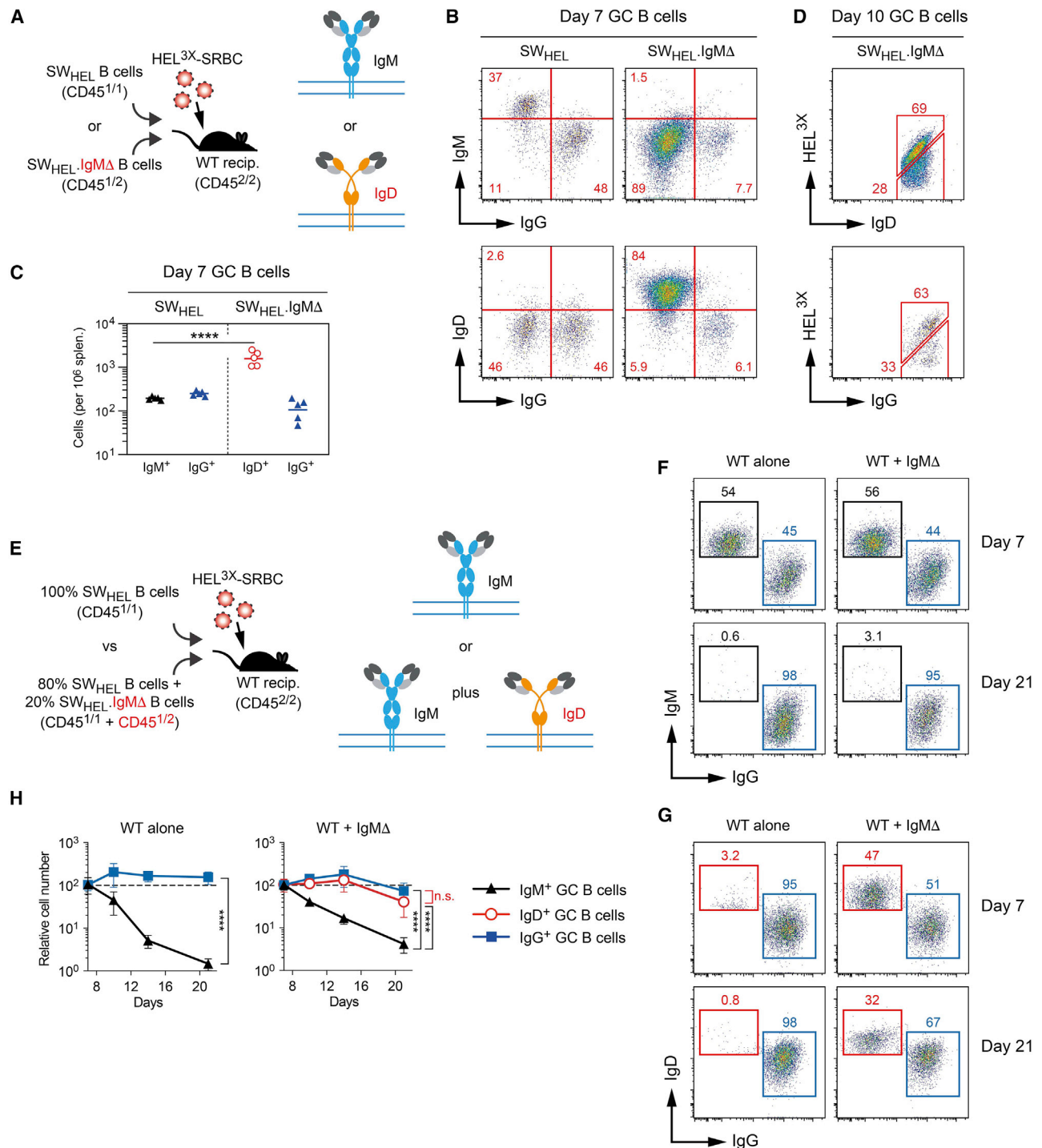


Figure 6. Expression of IgD instead of IgM prevents counter-selection of unswitched GC B cells

(A) Schematic of transfer experiment: wild-type SW_{HEL} ($CD45^{1/1}$) or $SW_{HEL}.IgM\Delta$ ($CD45^{1/2}$) B cells were transferred into $CD45^{2/2}$ wild-type recipients, challenged with HEL^{3X} -SRBC, and recipients analyzed from days 7 to 21.

(B) Representative flow cytometry plot showing proportion of unswitched IgM^+ or IgD^+ versus IgG -switched GC B cells from SW_{HEL} and $SW_{HEL}.IgM\Delta$ B cell responses on day 7.

(C) Numbers of IgM^+ , IgD^+ , and IgG^+ GC B cells derived from SW_{HEL} and $SW_{HEL}.IgM\Delta$ B cell responses on day 7. Data show individual mice and group means. p values were calculated using unpaired Student's t test; **** $p < 0.0001$.

(D) Representative flow cytometry plots showing affinity maturation (high-affinity HEL^{3X} -binding) of both IgD^+ and IgG^+ GC B cells derived from $SW_{HEL}.IgM\Delta$ B cell responses on day 10.

(legend continued on next page)

To establish GC responses containing IgM⁺, IgG⁺, and IgD⁺ GC B cells, recipient mice were injected with a spleen cell mixture made up of 20% SW_{HEL}.IgMΔ and 80% wild-type SW_{HEL} donor B cells. Control recipients received 100% wild-type SW_{HEL} B cells (Figure 6E). Day 7 GC responses formed in recipients of the 20:80 donor B cell mix contained similar frequencies of IgM⁺, IgG⁺, and IgD⁺ GC B cells (Figures 6F and 6G). As expected, donor-derived IgM⁺ GC B cells were virtually absent from both sets of recipients on day 21 (Figures 6F, 6H, and S4D). However, in recipients of 20% SW_{HEL}.IgMΔ donor B cells, IgD⁺ B cells still comprised approximately 30% of the GC at this late time point (Figures 6G, 6H, and S4D). Thus, counter-selection within the GC was not an innate property of all unswitched GC B cells but was specifically associated with expression of surface IgM. This result indicated that the basis of positive selection of switched versus unswitched GC B cells is explained through feature(s) present in IgG, but not IgM, BCRs. Moreover, the persistence of unswitched SW_{HEL}.IgMΔ B cells in the GC suggests that such feature(s) are also shared by IgD BCRs.

DISCUSSION

Positive selection of high-affinity B cells has long been recognized as the *raison d'être* of the GC and the fundamental mechanism driving antibody affinity maturation. Here, we describe a second mode of positive selection based on the BCR constant region, providing a new perspective on how the GC shapes humoral immunity. These findings help to explain the paradox of how antibody responses transition from IgM to IgG when class switching is known to cease upon GC formation. Thus, in addition to retaining high-affinity B cells, GC responses also selectively retain B cells that have previously switched to IgG. Together, these complementary processes of GC B-cell-positive selection promote the production of high-affinity IgG antibodies that define mature serum antibody responses.

Although positive selection of IgG⁺ GC B cells almost certainly contributes the predominance of IgG antibodies in mature antibody responses, it is likely reinforced by other complementary mechanisms. The early plasmablast response that occurs independent of the GC response is dominated by the production of IgM as opposed to IgG antibodies (Chan et al., 2009). However, as we demonstrated here, these IgM antibodies are typically low affinity and fail to persist due to the short-lived nature of plasmablasts. Furthermore, in addition to demonstrating positive selection of IgG⁺ GC B cells, analysis of responses from SW_{HEL} B cells carrying the Blimp1-GFP reporter gene revealed that IgG⁺ GC B cells showed a greater propensity to differentiate into PCs than their IgM⁺ counterparts. Similar to high- versus low-affinity GC B cells, therefore (Kräutler et al., 2017; Phan et al., 2006), IgG⁺

GC B cells can both persist and differentiate into PCs more readily than IgM⁺ GC B cells. This not only reinforces the dominance of IgG antibodies in the mature serological responses but suggests that the stimuli that preferentially select high-affinity and IgG⁺ B cells may be fundamentally similar.

We postulate, therefore, that the mechanisms responsible for positive selection of high-affinity B cells also drive positive selection of IgG⁺ B cells. This proposition is supported by our findings that, as was evident for high- versus low-affinity GC B cells, IgG⁺ GC B cells were more frequently in cell cycle and had a greater presence in the DZ compared to IgM⁺ GC B cells. Interestingly, positive selection of IgG⁺ over IgM⁺ GC B cells was more apparent among high-affinity as opposed to low-affinity GC B cells. Because the Y53D⁺ high-affinity cells identified in our study through staining with HEL^{3X} (at 50 ng/mL) have ~100-fold greater affinity than low-affinity cells carrying the original HyHEL10 specificity (Chan et al., 2012), it is possible that the low-affinity GC B cells as defined in this system fail to gain any significant access to FDC-displayed HEL^{3X} antigen and so cannot gain any advantage through expressing IgG BCRs. This may well be different when GC B cells have a range of more comparable affinities and so are in fact able to compete for antigen access.

The basis for the superior positive selection of IgG⁺ over IgM⁺ GC B cells remains unclear. Our results clearly indicate that the extended cytoplasmic domain carried by IgG, but not IgM, BCRs does not explain this phenomenon. This was underscored by the fact that GC B cells expressing IgD, which like IgM lacks an extended cytoplasmic domain, persisted within the GC as efficiently as IgG⁺ B cells. The fact that IgG and IgD, but not IgM, BCRs carry extended hinge domains raises the possibility that this structure may play a role in mediating constant region-based positive selection in the GC. The extended structure of the hinge domain is known to impart extra flexibility to IgG antibodies and therefore a greater ability to simultaneously engage epitopes with both Fab arms to form high-avidity complexes with antigen (Huber et al., 1976; Sapphire et al., 2002; Smith et al., 1993; Ye et al., 2016). In the context of the BCR, this may translate into membrane IgG having a superior ability to engage stably with the limiting depots of antigen displayed on FDCs compared to membrane IgM of equivalent affinity. Analysis of the contribution of the hinge and other features possessed by IgG, but not IgM, BCRs will be an important area of future work.

The lack of an obvious role for the IgG1 cytoplasmic tail in the positive selection of IgG1⁺ GC B cells was somewhat surprising, given the extensive literature identifying specific signaling and response modification properties associated with this domain (Engels et al., 2009; Horikawa et al., 2007; Kaisho et al., 1997; Martin and Goodnow, 2002). Although it is not clear whether

(E) Schematic of co-transfer experiment: wild-type SW_{HEL} (CD45^{1/1}) B cells were transferred either alone or in an 80:20 mix with SW_{HEL}.IgMΔ (CD45^{1/2}) B cells into CD45^{2/2} wild-type recipients, challenged with HEL^{3X}-SRBC, and recipients analyzed from days 7 to 21.

(F) Representative flow cytometry plots showing contributions of IgM⁺ and IgG⁺ B cells to GC responses derived from wild-type SW_{HEL} B cells transferred either alone or together with SW_{HEL}.IgMΔ B cells. Data from GC B cells not expressing IgM or IgG are omitted.

(G) Representative flow cytometry plots showing the relative contributions of IgD⁺ and IgG⁺ B cells to GC responses derived from wild-type SW_{HEL} B cells transferred either alone or together with SW_{HEL}.IgMΔ B cells. Data from GC B cells not expressing IgD or IgG are omitted.

(H) Kinetics of IgM⁺, IgD⁺, and IgG⁺ GC B cell responses derived from SW_{HEL} B cells transferred either alone or together with SW_{HEL}.IgMΔ B cells expressed relative to day 7. Data show the mean ± SD of 5 mice per group, representative of two experiments. Statistics were calculated using two-way ANOVA followed by Bonferroni's post hoc test with ****p < 0.0001.

the cytoplasmic tail of IgG1 modulates antigen capture and presentation, this result could reflect a minimal role for BCR signals versus recruitment of Tfh cell help, as has been previously proposed (Victora et al., 2010). Another surprising result was the augmentation of BCR expression and early B cell responses associated with removing the cytoplasmic domain from IgG1 and the complementary effects when this domain was added to IgM BCRs. The impact upon BCR expression can be explained by the recent finding that ubiquitylation of lysine residues in the IgG1 cytoplasmic domain negatively regulates its cell surface expression (Kodama et al., 2020). However, results obtained in a previous line of mice in which the IgG1 cytoplasmic domain sequences were removed indicated that this resulted in reduced expression of cell surface IgG1 (Kaisho et al., 1997). One possible explanation for this difference is that the line produced by Kaisho et al. over 20 years ago via embryonic stem cell technology required the retention of a palindromic loxP site within the 3' UTR of the membrane γ 1 heavy chain gene, which may have impacted upon mRNA stability. With the advantage of CRISPR-Cas9 technology, we were able to prevent expression of IgG1's extended cytoplasmic tail via a single-nucleotide change. For this reason, we favor the conclusion that increased rather than decreased expression of IgG1 BCRs is the true impact of removing its extended cytoplasmic tail. In light of this, it is noteworthy that the levels of wild-type IgM and IgG1 expressed on GC B cells are closely matched. This homogeneity in BCR density among GC B cells is likely to be an important factor in ensuring that positive selection operates on the basis of antigen affinity and heavy constant region composition rather than surface BCR expression levels.

IgD BCRs are co-expressed with IgM on naive B cells where its major function appears to be to optimize early B cell responses (Noviski et al., 2018; Roes and Rajewsky, 1993; Sabouri et al., 2016; Übelhart et al., 2015). Although IgD is normally downregulated shortly after B cell activation, our observations of the GC responses of SW_{HEL}-IgM Δ B cells showed that IgD is capable of sustaining B cells for long periods within the GC. Whatever the precise reason is that IgD⁺, but not IgM⁺, B cells can compete with IgG⁺ B cells in the GC, it is possible that the removal of IgD expression early in the response is important for ensuring that unswitched B cells are strongly counter-selected in the GC. Examination of responses from B cells in which the mechanism responsible for IgD suppression in the GC is inactivated will help to clarify this issue.

Although AID is required for both CSR and SHM, accumulating evidence indicates that only one of these activities occurs at any particular point during B cell differentiation. Thus, although B cells activated by various *in vivo* and *ex vivo* scenarios can undergo CSR, SHM occurs almost exclusively in GC B cells in which CSR is either infrequent or absent, as both we and others (Roco et al., 2019) have now established. As is outlined below, we propose that the restriction of AID activity to either CSR or SHM fundamentally shapes the organization and dynamics of *in vivo* B cell responses, including the requirement for BCR constant region-mediated selection in the GC.

To produce serum antibodies that are both high affinity and of the IgG class, naive antigen-specific B cells must go through at least two distinct phases in which either of the mutually exclusive processes of CSR or SHM predominates. Because the number of

possible outcomes from CSR is relatively small and occurs in a single, irreversible step, restricting this facet of AID activity to a short window prior to GC formation is sufficient to allow the generation of significant numbers of responding B cells that are IgG switched. However, as shown in this study, IgG⁺ B cells can be relatively infrequent in early GCs, meaning that the majority of GC B cells available to convert into “desirable” high-affinity specificities in fact carry the “undesirable” IgM class. With AID in GC B cells committed to ongoing rounds of SHM to generate effective, high-affinity specificities, a mechanism distinct from CSR is required to ensure that these specificities are ultimately linked to IgG rather than IgM antibodies. Thus, there is a clear requirement for an additional level of control in the GC response. We propose that this has been achieved by the evolution of constant region-based, positive selection of IgG⁺ GC B cells. In this way, a brief commitment of AID activity to CSR prior to GC formation stamps the appropriate Ig heavy chain isotype profile on a portion of responding B cells, which is subsequently amplified by constant region-based selection in the GC. This allows AID to focus predominantly on the more challenging and time-consuming task of generating high-affinity antibody specificities in ongoing GCs.

Limitations of study

We described positive selection of IgG⁺ GC B cells at the expense of IgM⁺ GC B cells in responses to two distinct antigens. It is possible, however, that GC responses in other contexts, for example, in active infections, may behave differently. It will be important to verify this in future studies, including whether CSR is always absent from GC B cells. The implication from our results that the hinge region of the BCRs is required for constant region-based positive selection of GC B cells also needs to be more rigorously tested. This could be done using a series of domain-swap mutants of IgG and IgM BCRs in an appropriate *in vivo* system. Finally, although recent single cell RNA sequencing (scRNA-seq) data are consistent with constant region-based selection also occurring in human GC B cell responses (King et al., 2021), it will be important to determine whether this is indeed the case.

STAR★METHODS

Detailed methods are provided in the online version of this paper and include the following:

- KEY RESOURCES TABLE
- RESOURCE AVAILABILITY
 - Lead contact
 - Materials availability
 - Data and code availability
- EXPERIMENTAL MODEL AND SUBJECT DETAILS
 - Mice
- METHOD DETAILS
 - Production of novel GM mouse lines using CRISPR/Cas9
 - Adoptive transfers and immunizations
 - Bone marrow chimeras
 - Anti-HEL^{3X} serum antibody ELISA
 - Antibodies, reagents and flow cytometry

- SHM analysis
- QUANTIFICATION AND STATISTICAL ANALYSIS

SUPPLEMENTAL INFORMATION

Supplemental information can be found online at <https://doi.org/10.1016/j.immuni.2021.03.013>.

ACKNOWLEDGMENTS

We thank staff of the Flow Cytometry Facility at the Garvan Institute for cell sorting, staff at Australian BioResources (ABR) for animal husbandry, and staff of Mouse Engineering Garvan/ABR (MEGA) for production of genetically modified CRISPR-Cas9 mice. Funding was from the National Health and Medical Research Council of Australia through a program grant and research fellowship to R.B. C.S. was supported by a postdoctoral fellowship from the Swedish Research Council (2013-7333).

AUTHOR CONTRIBUTIONS

Conceptualization, C.S. and R.B.; methodology, C.S., A.W.Y.L., K.B., C.Y., J.R.H., and D.Z.; validation, C.S., A.W.Y.L., K.B., C.Y., J.R.H., R.J.M., and R.B.; formal analysis, C.S., A.W.Y.L., K.B., C.Y., and R.B.; investigation, C.S., A.W.Y.L., K.B., and C.Y.; resources, R.B.; data curation, C.S., A.W.Y.L., and R.B.; writing—original draft, C.S., A.W.Y.L., and R.B.; writing—review and editing, C.S., A.W.Y.L., K.B., C.Y., J.R.H., D.B., N.J.K., D.Z., D.S., and R.B.; visualization, C.S., A.W.Y.L., C.Y., and R.B.; supervision, D.B., N.J.K., D.Z., D.S., and R.B.; project supervision, R.B.; funding acquisition, R.B.

DECLARATION OF INTERESTS

The authors declare no competing interests.

Received: September 21, 2020

Revised: December 29, 2020

Accepted: March 17, 2021

Published: April 14, 2021

REFERENCES

Berek, C., Berger, A., and Apel, M. (1991). Maturation of the immune response in germinal centers. *Cell* 67, 1121–1129.

Best, J.M., Banatvala, J.E., and Watson, D. (1969). Serum IgM and IgG responses in postnatally acquired rubella. *Lancet* 2, 65–68.

Borsos, T., and Rapp, H.J. (1965). Complement fixation on cell surfaces by 19S and 7S antibodies. *Science* 150, 505–506.

Brink, R., Goodnow, C.C., Crosbie, J., Adams, E., Eris, J., Mason, D.Y., Hartley, S.B., and Basten, A. (1992). Immunoglobulin M and D antigen receptors are both capable of mediating B lymphocyte activation, deletion, or anergy after interaction with specific antigen. *J. Exp. Med.* 176, 991–1005.

Brink, R., Paus, D., Bourne, K., Hermes, J.R., Gardam, S., Phan, T.G., and Chan, T.D. (2015). The SW(HEL) system for high-resolution analysis of in vivo antigen-specific T-dependent B cell responses. *Methods Mol. Biol.* 1297, 103–123.

Chan, T.D., Gatto, D., Wood, K., Camidge, T., Basten, A., and Brink, R. (2009). Antigen affinity controls rapid T-dependent antibody production by driving the expansion rather than the differentiation or extrafollicular migration of early plasmablasts. *J. Immunol.* 183, 3139–3149.

Chan, T.D., Wood, K., Hermes, J.R., Butt, D., Jolly, C.J., Basten, A., and Brink, R. (2012). Elimination of germinal-center-derived self-reactive B cells is governed by the location and concentration of self-antigen. *Immunity* 37, 893–904.

Ehrenstein, M.R., O’Keefe, T.L., Davies, S.L., and Neuberger, M.S. (1998). Targeted gene disruption reveals a role for natural secretory IgM in the maturation of the primary immune response. *Proc. Natl. Acad. Sci. USA* 95, 10089–10093.

Eisen, H.N., and Siskind, G.W. (1964). Variations in affinities of antibodies during the immune response. *Biochemistry* 3, 996–1008.

Engels, N., König, L.M., Heemann, C., Lutz, J., Tsubata, T., Griep, S., Schrader, V., and Wienands, J. (2009). Recruitment of the cytoplasmic adaptor Grb2 to surface IgG and IgE provides antigen receptor-intrinsic costimulation to class-switched B cells. *Nat. Immunol.* 10, 1018–1025.

Feng, Y., Seija, N., Di Noia, J.M., and Martin, A. (2020). AID in antibody diversification: there and back again. *Trends Immunol.* 41, 586–600.

Gitlin, A.D., Shulman, Z., and Nussenzweig, M.C. (2014). Clonal selection in the germinal centre by regulated proliferation and hypermutation. *Nature* 509, 637–640.

Goodnow, C.C., Crosbie, J., Adelstein, S., Lavoie, T.B., Smith-Gill, S.J., Brink, R.A., Pritchard-Briscoe, H., Wotherspoon, J.S., Loblay, R.H., Raphael, K., et al. (1988). Altered immunoglobulin expression and functional silencing of self-reactive B lymphocytes in transgenic mice. *Nature* 334, 676–682.

Horikawa, K., Martin, S.W., Pogue, S.L., Silver, K., Peng, K., Takatsu, K., and Goodnow, C.C. (2007). Enhancement and suppression of signaling by the conserved tail of IgG memory-type B cell antigen receptors. *J. Exp. Med.* 204, 759–769.

Huber, R., Deisenhofer, J., Colman, P.M., Matsushima, M., and Palm, W. (1976). Crystallographic structure studies of an IgG molecule and an Fc fragment. *Nature* 264, 415–420.

Hurwitz, J.L., Coleclough, C., and Cebra, J.J. (1980). CH gene rearrangements in IgM-bearing B cells and in the normal splenic DNA component of hybridomas making different isotypes of antibody. *Cell* 22, 349–359.

Jacob, J., Kelsoe, G., Rajewsky, K., and Weiss, U. (1991). Intraclonal generation of antibody mutants in germinal centres. *Nature* 354, 389–392.

Kaisho, T., Schwenk, F., and Rajewsky, K. (1997). The roles of gamma 1 heavy chain membrane expression and cytoplasmic tail in IgG1 responses. *Science* 276, 412–415.

Kallies, A., Hasbold, J., Tarlinton, D.M., Dietrich, W., Corcoran, L.M., Hodgkin, P.D., and Nutt, S.L. (2004). Plasma cell ontogeny defined by quantitative changes in blimp-1 expression. *J. Exp. Med.* 200, 967–977.

Khamlichi, A.A., Glaudet, F., Oruc, Z., Denis, V., Le Bert, M., and Cogné, M. (2004). Immunoglobulin class-switch recombination in mice devoid of any S mu tandem repeat. *Blood* 103, 3828–3836.

Kim, S., Davis, M., Sinn, E., Patten, P., and Hood, L. (1981). Antibody diversity: somatic hypermutation of rearranged VH genes. *Cell* 27, 573–581.

King, H.W., Orban, N., Riches, J.C., Clear, A.J., Warnes, G., Teichmann, S.A., and James, L.K. (2021). Single-cell analysis of human B cell maturation predicts how antibody class switching shapes selection dynamics. *Sci. Immunol.* 6, eabe6291.

Kodama, T., Hasegawa, M., Sakamoto, Y., Haniuda, K., and Kitamura, D. (2020). Ubiquitination of IgG1 cytoplasmic tail modulates B-cell signalling and activation. *Int. Immunol.* 32, 385–395.

Kräutler, N.J., Suan, D., Butt, D., Bourne, K., Hermes, J.R., Chan, T.D., Sundling, C., Kaplan, W., Schofield, P., Jackson, J., et al. (2017). Differentiation of germinal center B cells into plasma cells is initiated by high-affinity antigen and completed by Tfh cells. *J. Exp. Med.* 214, 1259–1267.

Mäkelä, O., Ruoslahti, E., and Seppälä, I.J. (1970). Affinity of IgM and IgG antibodies. *Immunochemistry* 7, 917–932.

Martin, S.W., and Goodnow, C.C. (2002). Burst-enhancing role of the IgG membrane tail as a molecular determinant of memory. *Nat. Immunol.* 3, 182–188.

Mayer, C.T., Gazumyan, A., Kara, E.E., Gitlin, A.D., Golijanin, J., Viant, C., Pai, J., Oliveira, T.Y., Wang, Q., Escolano, A., et al. (2017). The microanatomic segregation of selection by apoptosis in the germinal center. *Science* 358, eaao2602.

Muramatsu, M., Kinoshita, K., Fagarasan, S., Yamada, S., Shinkai, Y., and Honjo, T. (2000). Class switch recombination and hypermutation require activation-induced cytidine deaminase (AID), a potential RNA editing enzyme. *Cell* 102, 553–563.

Nimmerjahn, F., and Ravetch, J.V. (2007). Fc-receptors as regulators of immunity. *Adv. Immunol.* 96, 179–204.

- Noviski, M., Mueller, J.L., Satterthwaite, A., Garrett-Sinha, L.A., Brombacher, F., and Zikherman, J. (2018). IgM and IgD B cell receptors differentially respond to endogenous antigens and control B cell fate. *eLife* 7, e35074.
- Pape, K.A., Taylor, J.J., Maul, R.W., Gearhart, P.J., and Jenkins, M.K. (2011). Different B cell populations mediate early and late memory during an endogenous immune response. *Science* 331, 1203–1207.
- Paus, D., Phan, T.G., Chan, T.D., Gardam, S., Basten, A., and Brink, R. (2006). Antigen recognition strength regulates the choice between extrafollicular plasma cell and germinal center B cell differentiation. *J. Exp. Med.* 203, 1081–1091.
- Phan, T.G., Amesbury, M., Gardam, S., Crosbie, J., Hasbold, J., Hodgkin, P.D., Basten, A., and Brink, R. (2003). B cell receptor-independent stimuli trigger immunoglobulin (Ig) class switch recombination and production of IgG autoantibodies by anergic self-reactive B cells. *J. Exp. Med.* 197, 845–860.
- Phan, T.G., Paus, D., Chan, T.D., Turner, M.L., Nutt, S.L., Basten, A., and Brink, R. (2006). High affinity germinal center B cells are actively selected into the plasma cell compartment. *J. Exp. Med.* 203, 2419–2424.
- Plotkin, S.A., Orenstein, W.A., and Offit, P.A. (2008). *Vaccines*, Fifth Edition (Philadelphia, USA: Elsevier).
- Roco, J.A., Mesin, L., Binder, S.C., Nefzger, C., Gonzalez-Figueroa, P., Canete, P.F., Ellyard, J., Shen, Q., Robert, P.A., Cappello, J., et al. (2019). Class-switch recombination occurs infrequently in germinal centers. *Immunity* 51, 337–350.e7.
- Roes, J., and Rajewsky, K. (1993). Immunoglobulin D (IgD)-deficient mice reveal an auxiliary receptor function for IgD in antigen-mediated recruitment of B cells. *J. Exp. Med.* 177, 45–55.
- Sabouri, Z., Perotti, S., Spierings, E., Humburg, P., Yabas, M., Bergmann, H., Horikawa, K., Roots, C., Lambe, S., Young, C., et al. (2016). IgD attenuates the IgM-induced anergy response in transitional and mature B cells. *Nat. Commun.* 7, 13381.
- Saphire, E.O., Stanfield, R.L., Crispin, M.D., Parren, P.W., Rudd, P.M., Dwek, R.A., Burton, D.R., and Wilson, I.A. (2002). Contrasting IgG structures reveal extreme asymmetry and flexibility. *J. Mol. Biol.* 319, 9–18.
- Sharp, T.H., Boyle, A.L., Diebold, C.A., Kros, A., Koster, A.J., and Gros, P. (2019). Insights into IgM-mediated complement activation based on in situ structures of IgM-C1-C4b. *Proc. Natl. Acad. Sci. USA* 116, 11900–11905.
- Smith, T.J., Olson, N.H., Cheng, R.H., Chase, E.S., and Baker, T.S. (1993). Structure of a human rhinovirus-bivalently bound antibody complex: implications for viral neutralization and antibody flexibility. *Proc. Natl. Acad. Sci. USA* 90, 7015–7018.
- Steiner, L.A., and Eisen, H.N. (1967). Sequential changes in the relative affinity of antibodies synthesized during the immune response. *J. Exp. Med.* 126, 1161–1183.
- Suan, D., Kräutler, N.J., Maag, J.L.V., Butt, D., Bourne, K., Hermes, J.R., Avery, D.T., Young, C., Statham, A., Elliott, M., et al. (2017). CCR6 defines memory B cell precursors in mouse and human germinal centers, revealing light-zone location and predominant low antigen affinity. *Immunity* 47, 1142–1153.e4.
- Übelhart, R., Hug, E., Bach, M.P., Wossning, T., Dühren-von Minden, M., Horn, A.H., Tsiantoulas, D., Kometani, K., Kurosaki, T., Binder, C.J., et al. (2015). Responsiveness of B cells is regulated by the hinge region of IgD. *Nat. Immunol.* 16, 534–543.
- Uhr, J.W., and Finkelstein, M.S. (1963). Antibody formation. IV. Formation of rapidly and slowly sedimenting antibodies and immunological memory to bacteriophage phi-X 174. *J. Exp. Med.* 117, 457–477.
- Victoria, G.D., and Nussenzweig, M.C. (2012). Germinal centers. *Annu. Rev. Immunol.* 30, 429–457.
- Victoria, G.D., Schwickert, T.A., Fooksman, D.R., Kamphorst, A.O., Meyer-Hermann, M., Dustin, M.L., and Nussenzweig, M.C. (2010). Germinal center dynamics revealed by multiphoton microscopy with a photoactivatable fluorescent reporter. *Cell* 143, 592–605.
- White, M.B., Shen, A.L., Word, C.J., Tucker, P.W., and Blattner, F.R. (1985). Human immunoglobulin D: genomic sequence of the delta heavy chain. *Science* 228, 733–737.
- Yang, H., Wang, H., and Jaenisch, R. (2014). Generating genetically modified mice using CRISPR/Cas-mediated genome engineering. *Nat. Protoc.* 9, 1956–1968.
- Ye, X., Fan, C., Ku, Z., Zuo, T., Kong, L., Zhang, C., Shi, J., Liu, Q., Chen, T., Zhang, Y., et al. (2016). Structural basis for recognition of human enterovirus 71 by a bivalent broadly neutralizing monoclonal antibody. *PLoS Pathog.* 12, e1005454.

STAR★METHODS

KEY RESOURCES TABLE

REAGENT or RESOURCE	SOURCE	IDENTIFIER
Antibodies		
<i>InVivo</i> Ab anti-mouse CD16/CD32 (Clone 2.4G2)	BioXCell	Cat# BE0307; RRID: AB_2736987
PE/Cy7 anti-mouse CD45.2 Antibody (Clone 104)	BioLegend	Cat# 109830; RRID: AB_1186098
BUV395 Anti-Mouse CD45.2 (Clone 104)	BD Biosciences	Cat# 564616; RRID: AB_2738867
PerCP-Cy5.5 Mouse Anti-Mouse CD45.1 (Clone A20)	BD Biosciences	Cat# 560580; RRID: AB_1727489
FITC Mouse Anti-Mouse CD45.1 (Clone A20)	BD Biosciences	Cat# 553775; RRID: AB_395043
BV786 Rat Anti-Mouse CD45R/B220 (Clone RA3-6B2)	BD Biosciences	Cat# 563894; RRID: AB_2738472
PerCp-Cy5.5 Rat Anti-Mouse CD45R/B220 (Clone RA3-6B2)	BD Biosciences	Cat#552771; RRID: AB_394457
PE/Cy7 Rat Anti-Mouse CD38 (Clone 90)	eBioscience	Cat# 25-0381-82; RRID: AB_2573344
PerCp-Cy5.5 Rat Anti-Mouse CD38 (Clone 90)	BD Biosciences	Cat# 562770; RRID: AB_2737782
BV510 Rat Anti-Mouse CD38 (Clone 90)	BD Biosciences	Cat# 740129; RRID: AB_2739886
BV510 Hamster Anti-Mouse CD95 (Clone Jo2)	BD Biosciences	Cat# 563646; RRID: AB_2738345
Biotin Rat Anti-Mouse IgG1 (Clone A85-1)	BD Biosciences	Cat# 550331; RRID: AB_2296342
Biotin Anti-Mouse IgG2b (Clone RMG2b-1)	BioLegend	Cat# 406704; RRID: AB_315067
Biotin Mouse Anti-Mouse IgG2a[b] (Clone 5.7)	BD Biosciences	Cat# 553504; RRID: AB_394889
Biotin Rat Anti-Mouse IgG3 (Clone R40-82)	BD Biosciences	Cat# 553401; RRID: AB_394838
Biotin Anti-Mouse IgM[b] (Clone AF6-78)	BioLegend	Cat# 406204; RRID: AB_315037
PE Anti-Mouse IgM[b] (Clone AF6-78)	BioLegend	Cat# 406208; RRID: AB_315041
PE Anti-Mouse IgM[a] (Clone DS-1)	BD Biosciences	Cat# 553517; RRID: AB_394898
FITC Anti-Mouse IgM[a] (Clone DS-1)	BD Biosciences	Cat# 553516; RRID: AB_394897
FITC Rat Anti-Mouse IgD (Clone 11-26c.2a)	BD Biosciences	Cat# 553439; RRID: AB_394859
APC Rat Anti-Mouse IgD (Clone 11-26c.2a)	BD Biosciences	Cat# 565348; RRID: AB_2739201
BV650 Rat Anti-Mouse CD86 (Clone GL1)	BD Biosciences	Cat# 564200; RRID: AB_2738665
BV421 Rat Anti-Mouse CD184 (Clone 2B11/CXCR4)	BD Biosciences	Cat# 562738; RRID: AB_2737757
Biotin Rat Anti-Mouse CXCR4, Clone 2B11	BD Biosciences	Cat# 551968; RRID: AB_394307
PECy7 anti-mouse CD196 (CCR6) (Clone 29-2L17)	BioLegend	Cat# 129814; RRID: AB_1877147
PE Anti-Mouse CD196 (CCR6), Clone 29-2L17	BioLegend	Cat# 129803; RRID: AB_1279139
PE/Cy7 Hamster Anti-Mouse CD95 (clone Jo2)	BD Biosciences	Cat# 557653; RRID: AB_396768
BV510 Hamster Anti-Mouse CD95 (clone Jo2)	BD Biosciences	Cat# 563646; RRID: AB_2738345
Alexa Fluor 647 Hamster Anti-Mouse CD95 (clone Jo2)	BD Biosciences	Cat# 563647; RRID: AB_2738346
FITC Rat Anti-Mouse IgG1, Clone A85-1	BD Biosciences	Cat# 553443; RRID: AB_394862
PE Rat Anti-Mouse IgG1 (Clone A85-1)	BD Biosciences	Cat# 550083; RRID: AB_393553

(Continued on next page)

Continued

REAGENT or RESOURCE	SOURCE	IDENTIFIER
Purified Mouse anti-HEL, Clone HyHEL9	UCSF Monoclonal Antibody Core	Cat# AM033
BV421 Streptavidin	BD Biosciences	Cat# 563259; RRID: AB_2869475
PE/Cy7 Streptavidin	BD Biosciences	Cat# 557598; RRID: AB_I0049577
BV786 Streptavidin	BD Biosciences	Cat# 563858; RRID: AB_2869529
BUV395 Streptavidin	BD Biosciences	Cat# 564176; RRID: AB_2869553

Chemicals, peptides, and recombinant proteins

Recombinant HEL ^{3X} protein	Paus et al., 2006	N/A
Lysozyme from chicken egg white	Sigma-Aldrich	Cat# L6876-10G
Bovine pancreatic deoxyribonuclease I (DNase I)	Sigma-Aldrich	Cat#11284932001
DEPC treated DNase/RNase free water	Invitrogen	Cat# 46-2224
Proteinase K	Promega	Cat# V3021
Deoxynucleotide Mix	Sigma-Aldrich	Cat# D7295-.5ML
Taq DNA polymerase recombinant	Invitrogen	Cat# 100021276
SYBR Safe DNA Gel Stain	Invitrogen	Cat# S33102
illustra ExoStar 1-Step	VWR/ Bio-Strategy Limited	Cat# GEHEUS77705
Streptavidin, Alkaline Phosphatase Conjugate	ThermoFisher	Cat# S921
p-Nitrophenyl phosphate disodium hexahydrate	Sigma-Aldrich	Cat# 71768-25G
R-phycoerythrin	ProZyme/Agilent	Cat# PB32
Imject Alum Adjuvant (Pierce)	ThermoFisher	Cat# 77161

Critical commercial assays

FITC BrdU Flow Kit	BD Biosciences	Cat# 557891
FITC Active Caspase-3 Apoptosis Kit	BD Biosciences	Cat# 550480
Alexa Fluor 647 Antibody Labeling Kit	Life Technologies	Cat# A20186

Experimental models: organisms/strains

Mouse: C57BL/6JAusb	Australian BioResources	https://www.abr.org.au/animals/inbred-mice
Mouse: B6.SJL- <i>PtprcaPepcb</i> /BoyJAusb (CD45.1 congenic)	Australian BioResources	https://www.abr.org.au/animals/congenic-mice
Mouse: SW _{HEL} Ig transgenic	Phan et al., 2003	N/A
Mouse: MD4 Ig transgenic	Goodnow et al., 1988	N/A
Mouse: <i>Prdm1^{gfp}</i>	Kallies et al., 2004	N/A
Mouse: SW _{HEL} .IgG1cytΔ	This paper	N/A
Mouse: SW _{HEL} .IgMG1	This paper	N/A
Mouse: SW _{HEL} .IgMΔ	This paper	N/A
Mouse: SμΔ	This paper	N/A

Oligonucleotides

Primary SHH Upper (gtt gta gcc taa aag atg atg gtg)	Paus et al., 2006	Sigma-Aldrich
Primary SHH Lower (gat aat cgt tcc taa agg ctc tga g)	Paus et al., 2006	Sigma-Aldrich
Secondary SHH Upper (tct tct gta cct gtt gac agc cc)	Paus et al., 2006	Sigma-Aldrich
Secondary SHH Lower (caa ctt ctc tca gcc ggc tc)	Paus et al., 2006	Sigma-Aldrich

Software and algorithms

Flowjo software Version 9.9.6	Tree Star	https://www.flowjo.com/
GraphPad Prism Version 8.0	GraphPad	https://www.graphpad.com/scientific-software/prism/s

(Continued on next page)

Continued

REAGENT or RESOURCE	SOURCE	IDENTIFIER
Biostrings Bioconductor package Version 3.5	Bioconductor	http://www.bioconductor.org/packages/release/bioc/html/Biostrings.html
Photoshop CS6	Adobe	http://www.adobe.com/au/products/photoshop.html
Other		
Sheep red blood cells	Alsevers	Cat# SHBA0050
Normal mouse serum	Jackson ImmunoResearch	Cat# 015-000-120

RESOURCE AVAILABILITY

Lead contact

Further information and requests for resources and reagents should be directed to and will be fulfilled by the Lead Contact, Robert Brink (r.brink@garvan.org.au).

Materials availability

Genetically modified mouse lines generated in this study are available upon request and completion of a routine MTA.

Data and code availability

The published article includes all datasets generated or analyzed during this study. This study did not generate codes.

EXPERIMENTAL MODEL AND SUBJECT DETAILS

Mice

All genetically modified (GM) mouse lines were maintained on an inbred C57BL/6J background. SW_{HEL} (Phan et al., 2003) and MD4 (Goodnow et al., 1988) transgenic mice that produce B cells carrying the HyHEL10 specificity were generated as previously described. Both were crossed with the B6.SJL-*Ptprc*^a *Pepc*^b/BoyJ congenic line to become homozygous for the CD45.1 marker (*Ptprc*^{a/a}, depicted as CD45^{1/1} hereonin). SW_{HEL} mice were also crossed with *Prdm1*^{gfp} mice (Kallies et al., 2004) to generate a Blimp1-GFP (plasma cell) reporter line (SW_{HEL}.*Prdm1*^{gfp/+}.CD45^{1/1}). The novel GM mouse line S_μΔ (μ heavy chain switch-region deletion, Figure S1E) was produced using CRISPR/Cas9 technology in wild-type C57BL/6J embryos. Three additional novel GM mouse lines were produced using embryos heterozygous for the HyHEL10 VDJ-targeted Ig heavy chain gene of the SW_{HEL} line (Phan et al., 2003). These were SW_{HEL}.IgG1cytΔ (lacking the extended cytoplasmic tail of membrane γ1 heavy chain, Figure S4A), SW_{HEL}.IgM-cytG1 (adding the cytoplasmic domain of γ1 heavy chain to the μ heavy chain, Figure S3D) and SW_{HEL}.IgMΔ (lacking entire μ heavy chain gene, Figure S4A). Details of the production of GM lines are in the following section. Wild-type and CD45^{1/1} congenic (B6.SJL-*Ptprc*^a *Pepc*^b/BoyJ) C57BL/6J mice were obtained from Australian BioResources (Moss Vale, Australia). All recipient mice were male, were aged 6–12 weeks, were healthy, and had not been involved in previous procedures. All mice were bred and maintained in specific pathogen-free conditions at Australian BioResources and the Garvan Institute of Medical Research Biological Testing Facility. Animal experiments were performed under the approved guidelines of the Garvan Institute of Medical Research/St. Vincent's Hospital Animal Ethics Committee.

METHOD DETAILS

Production of novel GM mouse lines using CRISPR/Cas9

Novel GM mouse lines were produced by the Mouse Engineering Garvan/ABR (MEGA) Facility (Moss Vale and Sydney, Australia) by CRISPR/Cas9 gene targeting in C57BL/6J mouse embryos following established molecular and animal husbandry techniques (Yang et al., 2014). Embryos for microinjection were produced by mating stud males with super-ovulated C57BL/6J females. Stud males were either wild-type C57BL/6J mice or CD45^{1/1} congenic mice that were homozygous for the HyHEL10 VDJ-targeted Ig heavy chain gene of the SW_{HEL} line (Phan et al., 2003). All embryos were microinjected with *in vitro* transcribed and polyadenylated mRNA encoding *S.pyogenes* Cas9 and either one or two *in vitro* transcribed sgRNAs. Microinjected embryos were cultured overnight and introduced into pseudo-pregnant foster mothers. Pups were screened by PCR and Sanger sequencing of ear-punch DNA to identify founder mice which were then crossed to C57BL/6J or CD45^{1/1} congenic mice to establish each line. For modifications of the SW_{HEL} heavy chain gene, lines in which pups co-inherited this allele together with the novel engineered mutation were perpetuated.

To generate S_μΔ mice, two sgRNAs were used that targeted either side of the μ heavy chain switch-region (S_μ) sequence. The founder mouse carried a 1,713bp deletion including all 197 of the G(A/G)GCT repeat sequences present in S_μ (Figure S1E). To generate SW_{HEL}.IgG1cytΔ mice, an sgRNA was utilized whose associated “TGG” PAM corresponded to the tryptophan (W) codon

encoding the fourth amino acid residue of the cytoplasmic domain of the γ 1 membrane heavy chain gene (Figure S3A). A homologous recombination substrate was co-injected that comprised a single stranded sense 150 base PAGE-purified deoxy-oligonucleotide (IDT, Singapore) identical to the targeted locus except for a single nucleotide change converting the tryptophan codon into stop codon (TGG > TGA) (Figure S3A). Founder mice carried only this single nucleotide alteration to the *Ighg1* gene of the SW_{HEL} Ig heavy chain allele. To generate SW_{HEL}.IgMcytG1 mice, an sgRNA was utilized that targeted Cas9 cleavage 6 bp 3' of the stop codon of the μ membrane heavy chain cytoplasmic domain (Figure S3D). The co-injected, single stranded, sense deoxy-oligonucleotide homologous recombination substrate comprised sequence encoding the 25 aa extension of the IgG1 cytoplasmic domain flanked by sequences homologous to the *Ighm* gene that mediated insertion of the IgG1 sequence immediately prior to the stop codon of the μ membrane heavy chain gene cytoplasmic domain (Figure S3D). To generate SW_{HEL}.IgM Δ mice, two sgRNAs were used that targeted either side of the coding sequences and 3' polyadenylation sites of the *Ighm* gene (Figure S4A). The founder mouse carried a 6,231 bp deletion in the SW_{HEL} Ig heavy chain allele that removed all μ heavy chain coding sequences but retained the 5' switch-region (S μ) sequence (Figure S4A).

Adoptive transfers and immunizations

Recombinant HEL^{3X} protein was expressed as previously described (Paus et al., 2006). For experiments examining HEL-specific B cell responses, HEL^{3X} was first conjugated to SRBC (HEL^{3X}-SRBC) (Brink et al., 2015) then injected at 2×10^8 cells with 3×10^4 HEL-binding B cells per mouse into wild-type C57BL/6J recipient mice via i.v. (tail vein) injection. Polyclonal responses to SRBC were established via 2×10^8 SRBC i.v. and PE-specific responses were established through i.p. injection with 15 μ g R-phycoerythrin/PE (Prozyme) formulated in Alum (Pierce) in wild-type C57BL/6J mice. In experiments measuring cellular proliferation (BrdU incorporation), recipient mice were injected i.v. with 1 mg BrdU in 200 μ L PBS 1 h prior to sacrifice.

Bone marrow chimeras

Recipient wild-type CD45^{1/1} congenic mice of 8-12 weeks old were lethally irradiated (2×425 cGy) using an X-RAD 320 Biological Irradiator (Precision X-Ray, North Branford, CT). Femoral, humeral and tibial bone marrow cells from donor mice were aspirated into complete R10 media (10% FCS, 55 mM β -mercaptoethanol, 50 units/mL penicillin, 50 mg/mL streptomycin in RPMI). Single cell suspensions consisting of a 50:50 mixture of bone marrow cells from wild-type CD45^{1/1} congenic mice and either wild-type or S μ Δ CD45^{2/2} mice were injected i.v. into recipient mice 15 h post-irradiation (10^7 nucleated cells per recipient). The resulting chimeras were used for experiments after reconstituting for 8-10 weeks.

Anti-HEL^{3X} serum antibody ELISA

ELISA detection of HEL^{3X}-binding serum antibodies was performed as described (Brink et al., 2015). Briefly, 384-well plates (Corning) were coated with 10 μ g/mL HEL^{3X} and blocked with 1% BSA. Serially diluted serum samples were then incubated on the plates and bound antibodies subsequently detected with biotinylated anti-IgM or anti-IgG1 mAbs followed by streptavidin-alkaline phosphatase, p-nitrophenyl phosphate substrate and colorimetric spectrophotometry at 405 nm.

Antibodies, reagents and flow cytometry

Splenic samples were dissociated into single cell suspensions in complete R10 media (10% FCS, 55 mM β -mercaptoethanol, 50 units/mL penicillin, 50 mg/mL streptomycin in RPMI), red blood cell lysed and resuspended into 1% BSA supplemented with 0.1% azide in phosphate buffered saline (PBS). Cells were incubated with purified anti-mouse CD16/32 (2.4G2) and with either 50 ng/mL HEL^{3X} for affinity separation or 200 ng/mL HEL for enumeration of total HEL-specific B cell response. Cells were surface stained with mAbs targeting CD45.2 (104; BioLegend), CD45.1 (A20), CD45R/B220 (RA3-6B2) (both from eBiosciences), CD38 (90) CD95/Fas (Jo2) (both from BD Biosciences) to identify donor-derived GC B cells. GC B cell subpopulations were identified using anti-IgG1 (A85-1), IgG2b (RMG2b1), IgG2a^b (= IgG2c) (5.7), IgG3 (R40-82), IgM^b (AF6-78) (for SW_{HEL} or PE experiments) or IgM^a (DS-1) (for MD4 mice experiment), IgD (11-26c.2a), CD86 (GL-1), CXCR4 (2B11) (all from BD Biosciences). Anti-CCR6 (29-2L17, BioLegend) was used to identify for memory B cell precursors in the GC (Suan et al., 2017). HyHEL9 detection mAb was sourced from UCSF Hybridoma Core and fluorochrome-conjugated using the AlexaFluor 647 Protein Labeling Kit (Invitrogen) according to manufacturer's instructions to detect HEL-binding SW_{HEL} B cells. Detection of cellular proliferation and apoptosis was performed using the FITC BrdU Flow kit and anti-active caspase 3 mAb (C92-605), respectively (all BD Biosciences) according to the manufacturer's instructions. Labeled cells were analyzed using a BD LSRII SORP or BD LSR Fortessa with gating performed as previously described (Chan et al., 2012).

SHM analysis

Donor-derived SW_{HEL} GC B cells (CD45.1⁺, CD45.2⁻, B220^{hi}, CD38^{lo}, Fas^{hi}) from recipient spleens were sorted at single-cell density into 10 μ L lysis buffer containing 1X Taq PCR buffer, 0.5 mg/mL proteinase K, 0.1 mM EDTA, and 0.1% Tween-20 using a FACSAria cell sorter (BD Biosciences). The cells were then incubated at 56°C for 40 min, 95°C for 8 min and then frozen at -80°C. The HyHEL10 heavy chain variable region gene was then amplified by nested PCR and sequenced as described previously (Brink et al., 2015).

QUANTIFICATION AND STATISTICAL ANALYSIS

Data were analyzed using Microsoft Excel 2010 (Microsoft Corporation, Redmond), FlowJo™ v10 (FlowJo™ LLC, BD Biosciences) and BD FACSDiva v8.0.1 (BD Biosciences). Graphs for statistical analysis were generated using Prism Version 8.2.0 (GraphPad Software, San Diego, California, USA). For comparison between two groups, an unpaired Student's t test was used, while specific comparison with 3 or more groups was done using one-way ANOVA followed by a Bonferroni post-test. Where two variables were compared simultaneously, two-way ANOVA or a mixed-effects analysis was used followed by Bonferroni's or Dunnett's post-test. Kinetic data based on cell numbers was log₁₀-transformed prior to statistical analysis. A p value < 0.05 was considered significant, with *p < 0.05, **p < 0.01, ***p < 0.001, ****p < 0.0001. Individual data points in figures represent individual mice, while bar or line graphs show mean and standard deviation.